Journal of Medicinal Chemistry

pubs.acs.org/jmc

Article

Illuminating a Dark Kinase: Structure-Guided Design, Synthesis, and Evaluation of a Potent Nek1 Inhibitor and Its Effects on the Embryonic Zebrafish Pronephros

Georg Baumann,* Tobias Meckel, Kevin Böhm, Yung-Hsin Shih, Mirco Dickhaut, Torben Reichardt, Johannes Pilakowski, Ulrich Pehl, and Boris Schmidt*

Cite This: https://dx.doi.org/10.1021/acs.jmedchem.0c02118

Read Online

ACCESS | Metrics & More | Article Recommendations | Supporting Information

ABSTRACT: NIMA-related kinase 1 (Nek1) has lately garnered attention for its widespread function in ciliogenesis, apoptosis, and the DNA-damage response. Despite its involvement in various diseases and its potential as a cancer drug target, no directed medicinal chemistry efforts toward inhibitors against this dark kinase are published. Here, we report the structure-guided design of a potent small-molecule Nek1 inhibitor, starting from a scaffold identified by kinase cross-screening analysis. Seven lead compounds were identified *in silico* and evaluated for their inhibitory activity. The top compound, **10f**, was further profiled for efficacy, toxicity, and bioavailability in a zebrafish polycystic kidney disease model. Administration of **10f** caused the expansion of fluorescence-labeled proximal convoluted tubules, supporting our hypothesis that Nek1-inhibition causes cystic kidneys in zebrafish embryos. Compound **10f** displayed insignificant inhibition in 48 of 50 kinases in a selectivity test panel. The findings provide a powerful tool to further elucidate the function and pharmacology of this neglected kinase.

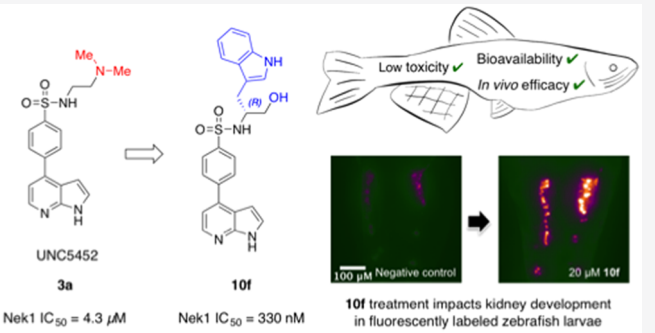

INTRODUCTION

Nek1 is a dual serine/threonine protein kinase that also possesses tyrosine kinase activity, albeit to a lesser degree.[1] Since its discovery in a murine cDNA expression library screen, this mammalian homologue of the fungal NIMA cell cycle regulator has attracted widespread attention due to its pleiotropic function and its association with a number of diseases in humans.[2−4] The ever-growing interest in this remarkable kinase was first sparked by findings that linked Nek1 to two independent mutant alleles (*kat* and *kat*^{2J}), which spontaneously arose from two inbred mouse strains, causing various effects such as male sterility, dwarfing, facial dysmorphism, anemia, and a progressive polycystic kidney disease (PKD).[5,6] PKD is the most common genetic cause for renal failure in humans and is characterized by the relentless growth of large fluid-filled cysts and the accompanying destruction of the adjacent renal parenchyma.[7] The evidence for the causative relation between Nek1 depletion and PKD was further strengthened by an interactomic study, which indicated strong interactions between the PKD-associated proteins KIF3A, tuberin, and α-catulin and the central coiled-coil region of Nek1.[8] Moreover, Nek1 expression levels are prominently elevated in embryonic proximal tubule and podocyte precursor cells and decrease with kidney maturation, supporting the observation that Nek1 is of functional importance for the etiology of PKD.[9]

Interestingly, NEK1 mutations have been linked not only to defects of ciliogenesis, like PKD and short-rib polydactyly syndrome type Majewski but also to other inheritable diseases such as Mohr−Laussen syndrome or amyotrophic lateral sclerosis (ALS), a neurodegenerative disorder that causes the selective death of motor neurons and is associated with an altered DNA damage response (DDR).[10−13] Like most of the 11 known members of the human Nek family, Nek1 plays a crucial role in cell cycle control and in particular the DDR.[14] Nek1 expression is upregulated upon chemical or radiative induction of DNA double-strand breaks (DSBs) and acts as a regulator of DNA repair by homologous recombination (HR).[15,16] Cell cycle phase-specific phosphorylation of Rad54 by Nek1 either permits HR, by way of Rad51 removal from chromatin in G2-phase, or ensures replication fork stability in S-phase.[17] Moreover, functional Nek1 is indispensable for proper cell cycle checkpoint activation through phosphorylation of checkpoint kinases 1 and 2 (Chk1/Chk2)

Special Issue: New Horizons in Drug Discovery - Understanding and Advancing Kinase Inhibitors

Received: December 8, 2020

in response to radiative stress.[18] Eventually, Nek1-deficient cells accumulate unrepaired DSBs leading to genomic instability, chromosomal damage, and finally cell death.[19] A remarkable feature of Nek1 is its ability to also limit apoptotic cell death even after severe damage has occurred already. Direct phosphorylation of voltage-dependent anion channel 1 (VDAC1) by Nek1 stabilizes the mitochondrial membrane potential thus limiting the caspase-mediated killing of cells.[20,21] More recent evidence suggests that an activating phosphorylation of Nek1 by tousled-like kinase 1 (Tlk1) contributes to the phosphorylation of VDAC1 and that inhibition of the Tlk1/Nek1/VDAC1 axis in combination with DNA damaging agents can sensitize prostate cancer cells to apoptotic killing.[22−25] Elevated levels of Nek1 expression have also been identified in other cancer types like thyroid cancer, human gliomas, or renal cell carcinoma (RCC).[26−28] In the latter case, a decreased sensitivity to genotoxic treatment and ionizing radiation was associated with high levels of Nek1, emphasizing the importance of Nek1 inhibition as a therapeutic strategy for drug development in the treatment of RCC.[28,29] More recently, Freund et al. have shown that high Nek1 expression levels associate with impaired clinical outcome in cervical cancer patients following chemo-radiotherapy or brachytherapy and that a Nek1 knockdown impacts the 3D clonogenic survival of HeLa cervical and HCT-15 colorectal carcinoma cells. Furthermore, the knockdown sensitized those cells to ionizing radiation, underlining the potential of Nek1 inhibitors to increase the radiation or chemotherapy response in anticancer treatment.[30]

Despite the crucial role of Nek1 in a broad variety of diseases and its outstanding potential as a target for anticancer therapeutics, no directed medicinal chemistry efforts toward potent and selective Nek1 inhibitors have been published in the past.[4,31] In a first attempt to pinpoint structural elements that influence Nek family inhibitor specificity, Moraes et al. identified a c-Jun N-terminal kinase (JNK) inhibitor with limited inhibitory activity against a truncated Nek1 activation loop mutant in a thermal shift assay.[32] Shortly thereafter, the same group reported the crystal structure analysis of the human Nek1 kinase domain both in its apo form and in complex with an ATP-competitive CDK inhibitor.[33] Until today, only three members of the human Nek family, namely, Nek1, -2, and -7, have been structurally solved. More recently, a pyridin-2(5*H*)-one based inhibitor with a low micromolar IC_{50} value against Nek6 was also shown to decrease Nek1 activity to a comparable degree.[35] In the framework of developing a comprehensive kinase chemogenomic set, Wells et al. compiled chemical starting points for Nek-family inhibitors by performing an intricate analysis of kinome cross-screening data.[34] In the case of Nek1, two series of compounds with promising activities were identified from the profiling data of a large inhibitor set (Published Kinase Inhibitor Set 2, PKIS2).[36] The most potent candidate (UNC5078) of a series of 4-thiophene-7-azaindoles exhibited 91.9% Nek1 inhibition at 1 μM.[34,37] Strikingly, the 4-aryl-7-azaindole derivative UNC5452 (**3a**), which was originally intended as an IκB kinase β (IKKβ) inhibitor, exhibited even higher Nek1 activity (99.8% inhibition at 1 μM) while only inhibiting 18 off-target kinases ≥90% at 1 μM (Figure 1).[34,38] Nevertheless, finding suitable inhibitors for Nek1 is not trivial, as indicated by the low hit rates of previously reported screenings.[33,34]

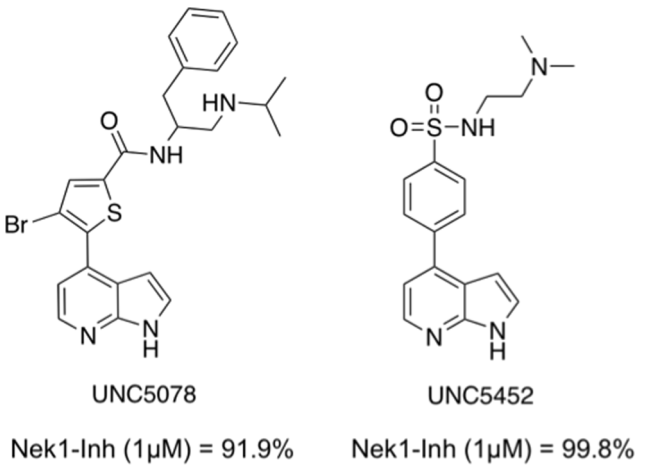

Figure 1. Chemical starting points for the development of Nek1 inhibitors, as identified by Wells et al. in an analysis of kinome cross-screening data.[34]

In this work, we report the structure-guided design and synthesis of several novel Nek1 inhibitors. The 4-phenyl-7-azaindole moiety of UNC5452 (**3a**) served as a starting point and was expanded upon by *in silico* analysis, molecular docking simulations, and a virtual chemical library screen in P-loop reconstructed Nek1 crystal structures (PDB codes 4APC and 4B9D) as well as a Nek1/Nek2 homology model. The most potent compound **10f** was further profiled in a kinase selectivity panel, a Caco-2 permeability assay, and a zebrafish developmental toxicity assay. *In vivo* efficacy of **10f** was evaluated by fluorescence microscopy imaging of zebrafish pronephroi after inhibitor treatment, which is an established model for cystic kidney diseases.[39]

CHEMISTRY

The synthesis of UNC5452 (**3a**) and its derivatives commenced with the amide formation between sulfonyl chloride **1** and the respective primary or secondary amines to afford sulfonamides **2a−h** and **2j−l**. Acetyloxyester **2i** was prepared from alcohol **2f** by acetylation with acetic anhydride. Miyaura borylation of aryl halides **2a−l** gave the corresponding pinacol boronic acid esters, which were fused with 4-bromo-7-azaindole by palladium catalyzed Suzuki cross-coupling forthwith, yielding 4-phenyl-7-azaindoles **3a−l** (Scheme 1).[40] In an attempt to synthesize the carboxylic amide analogue **6** of sulfonamide **2f** under identical conditions, 4-bromobenzoyl chloride (**4**) was transformed to the undesired ester **5**. However, alkaline hydrolysis of **5** provided benzamide **6**, which was coupled to 4-bromo-7-azaindole, giving azaindole **7** in the final Suzuki cross-coupling step. (Scheme 2). The amino alcohols **8a−f** were converted to final compounds **10a−f** through a similar sequence described in Scheme 1. Compounds **8a−c** were obtained commercially, while **8d** was prepared by reduction of D-tyrosine methyl ester with sodium borohydride and **8e** and **8f** were prepared by reduction of L-tryptophan and D-tryptophan, following a procedure by Meyers et al.[41,42] Amide formation between 4-bromosulfonyl chloride (**1**) and amino alcohols **8a−f** provided aryl halides **9a−f**, which again underwent Miyaura borylation and subsequent Suzuki cross-coupling to afford azaindoles **10a−f** (Scheme 3).

https://dx.doi.org/10.1021/acs.jmedchem.0c02118
J. Med. Chem. XXXX, XXX, XXX−XXX

Scheme 1[a]

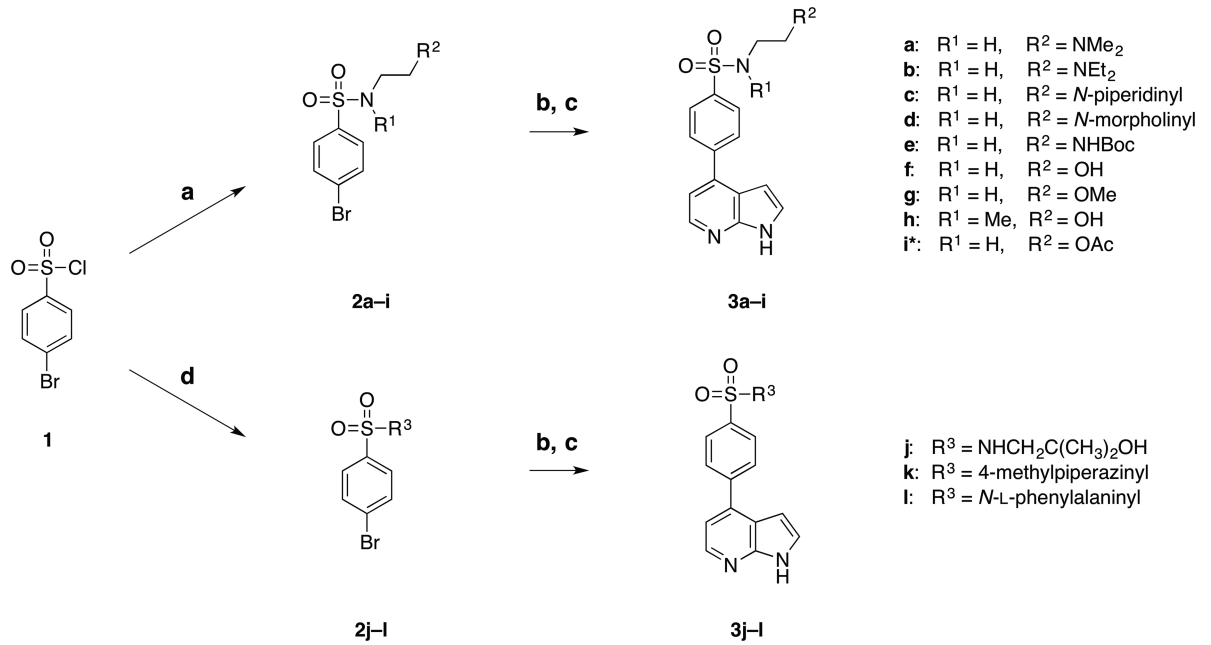

[a]Reagents and conditions: (a) for **2a–h**, DCM, amine, NEt_3, 0 °C–rt, 74–95%; (b) DMF, bis(pinacolato)diboron, KOAc, $PdCl_2$(dppf), 100 °C, not isolated; (c) DMF, 4-bromo-7-azaindole, $NaHCO_3$ (aq), $Pd(PPh_3)_4$, 100 °C, 11–69%; (d) for **2j**, DCM, amine, NEt_3, 0 °C–rt, 64%; for **2k**, THF, 1-methylpiperazine, rt, 75%; for **2l**, H_2O/acetone, L-phenylalanine, $NaHCO_3$, rt, 49%. *Compound **2i** was prepared from **2f** by acetylation with acetic anhydride and NEt_3 in DCM, 82%; see Experimental Section for more details.

Scheme 2[a]

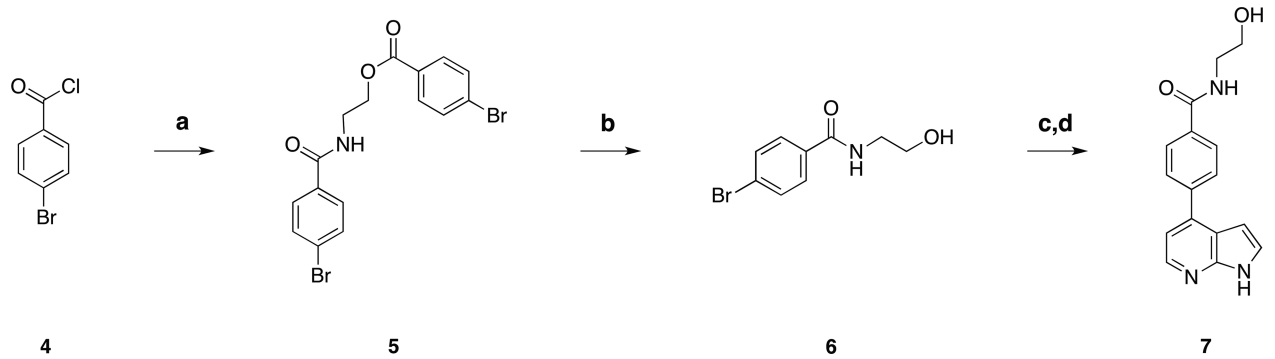

[a]Reagents and conditions: (a) DCM, monoethanolamine, NEt_3, 0 °C–rt, 48%; (b) THF, 50% w/v KOH (aq), 60 °C, 92%; (c) DMF, bis(pinacolato)diboron, KOAc, $PdCl_2$(dppf), 100 °C, not isolated; (d) DMF, 4-bromo-7-azaindole, $NaHCO_3$ (aq), $Pd(PPh_3)_4$, 100 °C, 43%; see Experimental Section for more details.

RESULTS AND DISCUSSION

Molecular Modeling. As an initial step of the structure-guided design, the available Nek1 kinase domain crystal structures were analyzed in detail. Both the apo (PDB code 4APC) and the CDK-inhibitor bound 3D structures (PDB code 4B9D) were obtained from the same inactivating T162A activation loop mutant and expectedly constitute an inactive "DFG-out/C-helix-out" conformation. The activation loop forms an ordered α helix, which is speculated to unfold upon autophosphorylation, thus adopting a disordered conformation more commonly found in active kinases.[33] This activation mechanism might to some degree be conserved in the Nek-family, as a similar α-helical activation loop was observed in Nek2 structures but not in Nek7, which is activated through a different mechanism that involves binding of the noncatalytic C-terminal domain of Nek9.[43,44] Moreover, the Nek1 structures both crystallized as disulfide bridged dimers.

In an attempt to identify areas of conformational mobility in the active site, we isolated and superimposed the monomeric kinase domains using the Molecular Operating Environment (MOE) software platform (Figure S1). Interestingly, the DFG-motif aspartate (D146) and the gatekeeper (M80) formed hydrogen bonds with an internal water molecule in the ATP binding site in all but one of the isolated chains (PDB code 4APC.A). In this particular case, the side chains of D146 and M80 extend outward in absence of the water molecule, thus opening a hydrophobic back-pocket toward the DFG-motif. This conformational mobility might be exploited by locking Nek1 in an inactive conformation with a small molecule inhibitor. In order to assess the ligand–protein interactions and the amenability of the back-pocket, we docked UNC5452

https://dx.doi.org/10.1021/acs.jmedchem.0c02118
J. Med. Chem. XXXX, XXX, XXX–XXX

Scheme 3[a]

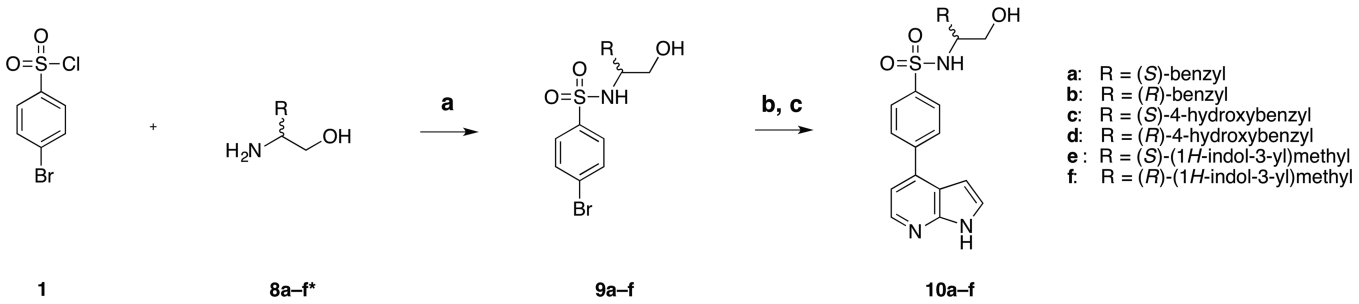

1 8a–f* 9a–f 10a–f

[a]Reagents and conditions: (a) for **9a**,**b**, DCM, amine, NEt_3, 0 °C−rt, 98−99%; for **9c**,**d**, H_2O/acetone, L-phenylalanine, $NaHCO_3$, rt, 60−70%; for **9e**,**f**, DCM/acetonitrile, *N*,*N*-diisopropylethylamine, 0 °C−rt, 30−43%; (b) DMF, bis(pinacolato)diboron, KOAc, $PdCl_2$(dppf), 100 °C, not isolated; (c) DMF, 4-bromo-7-azaindole, $NaHCO_3$ (aq), $Pd(PPh_3)_4$, 100 °C, 26−62%. *Compounds **8a−c** were obtained commercially; Compound **8d** was prepared from D-tyrosine methyl ester hydrochloride by freeing the amine with KOAc in acetonitrile and subsequent reduction with $NaBH_4$ in methanol, 61%; compounds **8e**,**f** were prepared by reduction of the corresponding tryptophan isomer using the method described by Meyers et al.,[41] 72−84%; see Experimental Section for more details.

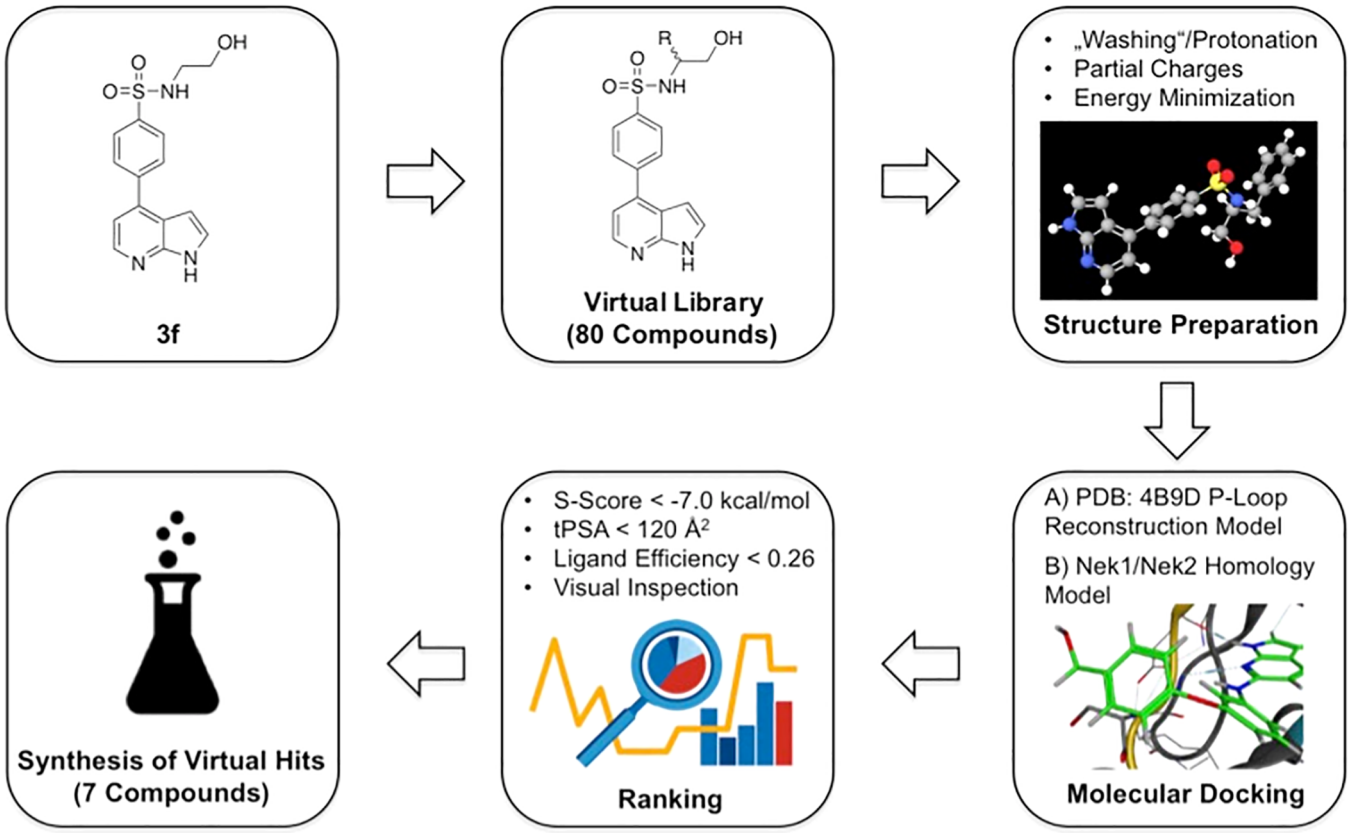

Figure 2. *In silico* chemical library screening to identify hit compounds. See Experimental Section for more details.

(**3a**) into the Nek1 ATP-binding site (PDB code 4APC.A, Figures S2 and S3).

The docking experiments suggest that the 7-azaindole moiety positions itself between V31 and F135 side chains and forms two hydrogen bonds with the backbone heteroatoms of the hinge region C83. The pyrrole ring is packed tightly against the side chain of Y82 and directed toward the solvent exposed area of the ATP-binding site, thus adopting the so-called "flipped" binding mode. The "normal" binding mode, where the pyrrole ring points toward the gatekeeper M80, is also conceivable but was not favored in our docking experiments.[45] From the hinge-binding motif, the phenyl ring of UNC5452 protrudes toward the ribose-binding region of Nek1 through a narrow channel formed by the side chains of F135, A18, I10, and the catalytic lysine (K33). Unfortunately, the terminal nitrogen atom of K33 is not structurally resolved, but it appears that its side-chain flexibility and the close proximity to the sulfonamide oxygen allow for hydrogen bonding. The proposed binding mode is supported by the 9-fold reduction of activity of carboxylic acid **7** against Nek1, when compared with sulfonamide **3f**. It appears that the tetrahedral geometry of the sulfonamide group is crucial for proper orientation of the ligand. Consequently, the sulfonamide nitrogen is positioned downward, toward the catalytic loop. As proposed by the docking experiment, the sulfonamide NH is not acting as a hydrogen bond donor, as the methyl

https://dx.doi.org/10.1021/acs.jmedchem.0c02118
J. Med. Chem. XXXX, XXX, XXX−XXX

substitution of the secondary sulfonamide hydrogen from **3f** to **3j** slightly increased potency.

As expected, the highly flexible dimethylaminoethyl fragment was able to adopt multiple conformations. Unfortunately, our experiments led to the conclusion that an entrance into the hydrophobic back pocket from the 4-phenyl-7-azaindole scaffold is not trivial. Due to the intrusion of the F135 and Y82 side chains into the hinge-binding region, the 7-azaindole moiety is angled in a way that hypothetically prevents access to the back-pocket from the 5-position in the "flipped" binding mode. In the disfavored "normal" binding mode, the same problem arises for the 3-position and an entry from the 2-position is presumably blocked by the gatekeeper (M80). Moreover, the docking shows that an approach from the ortho position of the scaffold's phenyl ring is likely also blocked by M80 (Figure S4). It remains unclear if scaffold hopping to a five membered aromatic ring as in UNC5078 would sufficiently widen the C−C−C bond angle to allow bypassing of the gatekeeper. Laufer and colleagues have successfully applied this strategy in the development of inhibitors for EGFR Met gatekeeper mutants in the past.[46]

As a consequence of these findings, we shifted our attention to the derivatization of the dimethylaminoethyl fragment with means to optimize existing and to establish new interactions in the ribose-binding region. Depending on the protonation state of the tertiary amine, interactions with the side chains of the catalytic loop residues D128 or Q132 or the unresolved side chains of the glycine-rich loop (P-Loop) residues E12 and S14 are conceivable. In order to establish a structure−activity relationship (SAR), we synthesized and evaluated compounds **3b−k**, with a range of steric demands as well as varying basicity and hydrogen bond capabilities. The most potent compound of the series, alcohol **3f**, served as the starting point for an *in silico* virtual library docking experiment to identify virtual hit compounds (Figure 2). We reasoned that the structural relation of the sulfonamide linked side chain to *N*-substituted α-amino acids and their corresponding alcohols allows us to make use of nature's own toolkit for protein binding. Moreover, this strategy ensured the convenient access to stereochemically pure starting materials and a straightforward synthetic approach.

The virtual library included a total of 80 compounds that correspond to both isomers of the 20 canonical amino acids and their respective amino alcohols. Molecular docking of the virtual library into the Nek1 kinase domain required reconstruction of the P-loop, which was performed using two independent methods. Starting from the ligand-bound B-chain (PDB code 4B9D), which was chosen because of its shorter unresolved gap, we first reconstructed the loop using the SuperLooper2 web application.[47] Second, a homology model of Nek1 was created using the X-ray structure of Nek2 bound to an aminopurine inhibitor (Figure S7).[48] Seven virtual hit compounds were identified by analysis of the docking results. The selection was based on docking score (*S*-Score), topological polar surface area (TPSA), ligand efficiency, and visual inspection of the docked conformations. Both methods provided similar results, favoring aromatic amino alcohol side chains (**10a−f**) and an aromatic amino acid side chain (**3l**).

Interestingly, the structurally related Nek1 kinase cross screening hit UNC5078 also possesses an equivalent benzyl group, although the stereoinformation is missing.[34] The putative binding mode of the series most potent compound **10f** was determined from molecular docking into the reconstructed X-ray structure of Nek1 (Figure 3). In similar fashion to **3a**, the 7-azaindole moiety is tightly packed between

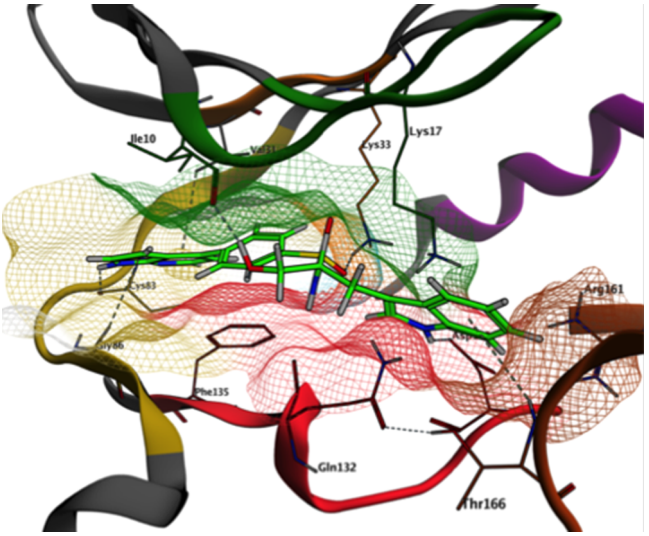

Figure 3. Molecular docking of compound **10f** into X-ray structure of Nek1 (PDB code 4B9D.B). P-loop reconstruction was performed using the SuperLooper2 web application.[47] See Experimental Section and Supporting Information for more details (Figures S5 and S6).

V31 and F135 in the "flipped" binding mode and forms two hydrogen bonds with the hinge region C83. Furthermore, the docking experiment indicates C−H−π interactions of the heterocyclic rings with G86 and V31 side chains as well as a contingent parallel-displaced $\pi-\pi$ stacking interaction with F135. The phenyl ring of **10f** once again protrudes toward the ribose binding region and positions the sulfonamide moiety in close proximity to the catalytic lysine (K33), forming a hydrogen bond. Resulting from this interaction, the hydroxyl group of **10f** acts as a hydrogen donor toward the backbone carbonyl oxygen of I10, while the indole moiety fits tightly between K17, Q132, and R161. From here, the indole NH forms a hydrogen bond with the side chain of D128, while the aromatic system establishes a C−H−π interaction with the T166 backbone NH. Judging by these results, **10f** can be classified as a type IIB inhibitor that binds to an inactive DFG-out conformation without occupying the back cleft.[49]

Biological Assays and Structure−Activity Relationship (SAR) Studies. As a first step, we synthesized UNC5452 (**3a**) in order to benchmark a commercial *in vitro* Nek1 activity assay by Eurofins Discovery (KinaseProfiler Item 15-020 KP10). Compound **3a** inhibited Nek1 activity by only 63% at 1 μM in this ATP-dependent radiometric assay, compared to the 99.8% inhibitory activity reported by Wells et al.[34] We hypothesize that this difference results from the fact that screening of the parent PKIS2 data set was performed using an ATP-independent competition-binding assay (DiscoverX KINOME-scan) that instead measures the ability of a small molecule to compete for the active site with an immobilized inhibitor.[36]

The molecular modeling suggested interactions of **3a** with the Nek1 hinge C83, catalytic K33, and the catalytic loop residues D128 and Q132 to be essential for potent inhibition. Since our primary aim was the optimization of the dimethylaminoethyl fragment, we first opted for the improvement of the terminal dimethylamino group. In the light of our

https://dx.doi.org/10.1021/acs.jmedchem.0c02118
J. Med. Chem. XXXX, XXX, XXX−XXX

docking experiments and the significant drop in activity upon removal of the two methyl groups, from **3a** to primary amine UNC5023 in the PKIS2 data set,[34] we investigated the influence of the amine pK_a by synthesis and evaluation of compounds **3b–e** (Table 1). Overall, the radiometric Nek1

Table 1. Inhibitory Activity of Compounds 3a–f and 3k against Nek1 and Nek2

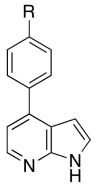		Residual kinase activity (1 μM)[a]	IC_{50} [μM][b]		
Cpd.	**R**	**Nek1**	**Nek1**	**95% CI**	**Nek2**
3a	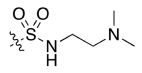	37%	7.1 (4.3)[c]	6.4 – 7.8 (3.1 – 5.9)[c]	n. e.
3b	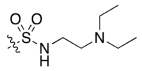	68%	10	9.6 - 11	n. e.
3c	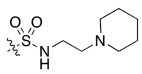	37%	6.6	6.3 – 6.9	n. e.
3d	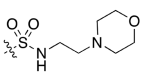	51%	27	17 - 62	n. e.
3e	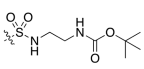	49%	n.e.	n.d.	n. e.
3f	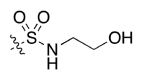	12%	3.2 (2.0)[c]	2.9 – 3.5 (1.4 – 2.8)[c]	n. e.
3k	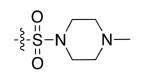	45%	>10[#]	n.d.	n. e.

[a]Eurofins Discovery KinaseProfiler service at 10 μM ATP. [b]LANCE Ultra TR-FRET kinase assay at $K_{m,ATP}$. [#]A relative IC_{50} value was provided because the determined IC_{50} value exceeded the employed maximum test concentration (10 μM). See Experimental Section for more details. See Supporting Information for raw data. CI, confidence interval; nd, not determined; ne, no effect at maximum concentration (30 μM). [c]Eurofins Discovery IC50Profiler service at $K_{m,ATP}$.

assay revealed no clear trend between the amine basicity and kinase binding. Compounds **3b**, **3d**, and **3e** displayed decreased activity in comparison to **3a**, while **3c** showed comparable activity. The results were confirmed by the determination of IC_{50} values for **3a–e** in a TR-FRET based Nek1 activity assay (LANCE Ultra TR-FRET, $K_{m,ATP}$, PerkinElmer). Strikingly, no effect on Nek1 activity was herein observed at the maximum concentration (30 μM) for **3e**, which reduced Nek1 activity to 49% in the radiometric assay. Furthermore, compound **3d** displayed a significant decrease in inhibitory activity compared to **3b**, in contrast to the previous findings. Apart from these discrepancies, the results confirm that a variation of the terminal amine's basicity did not improve inhibitory activity against Nek1. Rigidification of the flexible dimethylamino-ethyl fragment in compound **3k** also significantly decreased inhibitory activity against Nek1 to over 10 μM from 7.1 μM in **3a**. As a result, we reasoned that the attempted optimization of interactions of **3a** with the catalytic loop residues D128 and Q132, as suggested by the docking experiment, is elusive and that the introduction of an alternative hydrogen bond donor might improve inhibitory activity. Synthesis and evaluation of alcohol **3f** revealed a significant decrease in residual Nek1 activity to 12% as well as a more than 2-fold decreased IC_{50} of 3.2 μM, compared to **3a**.

In order to evaluate the hydrogen bond characteristics of the hydroxy group in **3f**, methyl ether **3g** and acetyl ester **3i** analogues were prepared and tested (Table 2). Both analogues

Table 2. Inhibitory Activity of Compounds 3g–j and 7 against Nek1 and Nek2

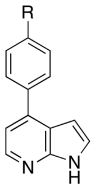		Residual kinase activity[a] (1 μM)	IC_{50} [μM][b]		
Cpd.	**R**	**Nek1**	**Nek1**	**95% CI**	**Nek2**
3g	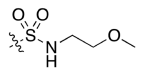	44%	>30[#]	n.d.	n. e.
3h	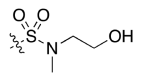	46%	2.7	2.5 – 3.0	n. e.
3i	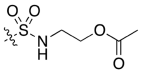	49%	8.8	7.0 - 11	n. e.
3j	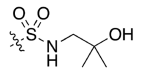	32%	5.8	4.7 – 7.2	n. e.
7	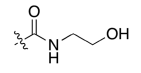	89%	29	25 - 35	n. e.

[a]Eurofins Discovery KinaseProfiler service at 10 μM ATP. [b]LANCE Ultra TR-FRET kinase assay at $K_{m,ATP}$. [#]A relative IC_{50} value was provided because the determined IC_{50} value exceeded the employed maximum test concentration (30 μM). See Experimental Section for more details. See Supporting Information for raw data. CI, confidence interval; nd, not determined; ne, no effect at maximum concentration (30 μM).

showed decreased inhibitory activity compared to **3f**, with an IC_{50} larger than 30 μM for ether **3g** and 8.8 μM for ester **3i**. The results clearly indicate that the hydroxy group in **3f** does indeed act as a hydrogen bond donor and not as an acceptor, as the reduced acceptor capability in **3i** did not further reduce inhibitory activity. It remains unclear if the carbonyl oxygen in **3i** acts as an alternative hydrogen bond acceptor but it is unlikely to interact with the same region, due to its different position relative to the rest of the molecule. Moreover, the introduction of a bulky tertiary alcohol in **3j** led to a significantly decreased IC_{50} of 5.8 μM. With the improved inhibitory activity of **3f** in hand, we switched our focus to the sulfonamide moiety (Table 2). As previously suggested by docking of **3a** into the Nek1 ATP binding site, the methyl replacement of the secondary sulfonamide hydrogen from **3f** to **3h** did not influence Nek1 inhibition significantly. However, substitution of the tetrahedral sulfonamide group with a planar carboxamide in **7** led to a 9-fold increased IC_{50} compared to **3f**,

https://dx.doi.org/10.1021/acs.jmedchem.0c02118
J. Med. Chem. XXXX, XXX, XXX–XXX

providing evidence for the proposed importance of the sulfonamide geometry in hydrogen bonding to K33. In addition, compounds **3a−k** and **7** were profiled for their Nek2 inhibitory activity using the same TR-FRET based assay platform. In concordance with the Nek-family selectivity data for **3a** reported by Wells et al.,[34] none of the tested compounds exerted an observable effect on the kinase activity of Nek2.

As described in the molecular modeling section, seven virtual hit compounds (**3l** and **10a−f**) were identified in an *in silico* screening from a library of canonical *N*-substituted *α*-amino acid derivatives, and their corresponding alcohols, structurally based on **3f**. Accordingly, phenylalanine derivative **3l** and phenylalaninol, tyrosinol, and tryptophanol derivatives **10a−f** were synthesized and evaluated (Table 3). The L-phenylalanine derivative **3l** did not notably decrease Nek1 activity, while the corresponding phenylalaninol derived enantiomers **10a** and **10b** displayed decreased Nek1 IC_{50} values of 1.9 μM and 1.3 μM, respectively. The tyrosinol derivatives **10c** and **10d** performed slightly worse, while the L-tryptophanol derivative **10e** exhibited a decreased IC_{50} compared to **10a** (0.99 μM). Strikingly, the D-tryptophanol derivative **10f** showed 6-fold decreased IC_{50} of 0.33 μM against Nek1 compared to **3f**. Our docking experiments suggest that this decrease results from the generally favored orientation of the (*R*)-enantiomers, which in this particular case gives rise to an additional hydrogen bond interaction of the indole NH with the D128 side chain as well as a C−H−π interaction of the aromatic system with the T166 backbone NH (Figure 3).

Kinase selectivity profiling of **10f** against 50 kinases was carried out with ATP concentrations set within 15 μM of the apparent K_m for ATP for each kinase tested, so that the resulting selectivity profile directly reflects the intrinsic affinities of **10f**.[50] Of the 50 kinases in this focused panel, including several members of the Nek family, 47 showed activity higher than 75%, whereas Nek1 displayed a residual activity of only 49.7%. The only kinase that was also significantly inhibited by **10f** was IKKβ with a residual activity of 36.1% (Figure 4). However, given that the selectivity profile is based on a limited number of kinases (approximately 10% of the kinome) and does not extend to enzymes beyond the kinome, caution must be exercised in deducing general selectivity from the data.

Zebrafish Developmental Toxicity Assay and Fluorescence Microscopy Imaging of Zebrafish Pronephroi. In order to evaluate whether its *in vitro* inhibitory activity translates into predictable effects *in vivo*, compound **10f** was further profiled for its activity, safety, and toxicity in wild-type zebrafish (*Danio rerio*). For this purpose, we established a PKD model based on a previously mentioned report by Chen et al., which indicates that Nek1 deficiency results in renal cyst formation as a consequence of disordered kidney maturation in *kat*^{2j} mice.[9] Indeed, the zebrafish has proven itself as an established model system for the evaluation of mammalian kidney morphology, because of its simple pronephric structure, which consists of two nephroi that share major anatomical and functional features with the mammalian metanephros. Its usefulness as a model for cystic kidney diseases has recently been reviewed.[39,51] Furthermore, it has been shown that the majority of human kinases display high degrees of identity with their zebrafish homologues. Human Nek1, for example, shares 89% identity to zebrafish Nek1 for the catalytically active kinase domain, according to a study by Wlodarchak et al.[52] Moreover, all residues of the active site appear unaltered in

Table 3. Inhibitory Activity of Compounds 3l and 10a−f against Nek1

	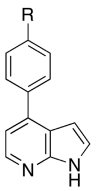	Residual kinase activity[a] (1 μM)	IC_{50} [μM][b]	
Cpd.	R	Nek1	Nek1	95% CI
3l	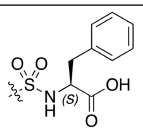	94%	n.e.	n.d.
10a	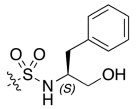	19%	1.9	1.4 - 2.6
10b	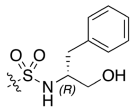	16%	1.3	0.91 – 1.8
10c	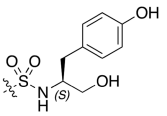	33%	2.0	1.2 – 3.0
10d	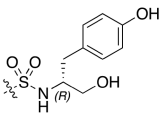	25%	1.6	1.1 – 2.2
10e	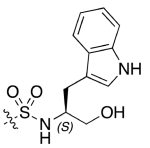	19%	0.99	0.65 – 1.5
10f	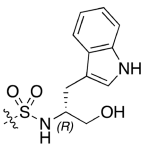	4%	0.33 (0.33)[c]	0.22 – 0.52 (0.19 – 0.51)[c]

[a]Eurofins Discovery KinaseProfiler service at 10 μM ATP. [b]Eurofins Discovery IC50Profiler service at $K_{m,ATP}$. See Experimental Section for more details. See Supporting Information for raw data. CI, confidence interval; nd, not determined; ne, no effect at maximum concentration (10 μM). [c]Eurofins Discovery IC50Profiler service at 10 μM ATP.

sequence analysis (Figures S8 and S9). We therefore hypothesized that treatment with **10f**, during early stages of embryonic organ development, leads to the formation of renal cysts, thus indicating efficient absorption and *in vivo* efficacy of **10f**. It is important to note here that our model is based on the necessary assumption that Nek1 inhibition results in the same phenotype that is associated with its depletion, as the correlation between small-molecule inhibition and loss-of-function phenotypes is not always straightforward.[53] However, our approach is substantiated by the reported link of aberrant cystic growth to the absence of Nek1, as well as to its overexpression.[54] Hence, the authors conclude that healthy ciliogenesis requires a delicate spatiotemporal activity of Nek1,

https://dx.doi.org/10.1021/acs.jmedchem.0c02118
J. Med. Chem. XXXX, XXX, XXX−XXX

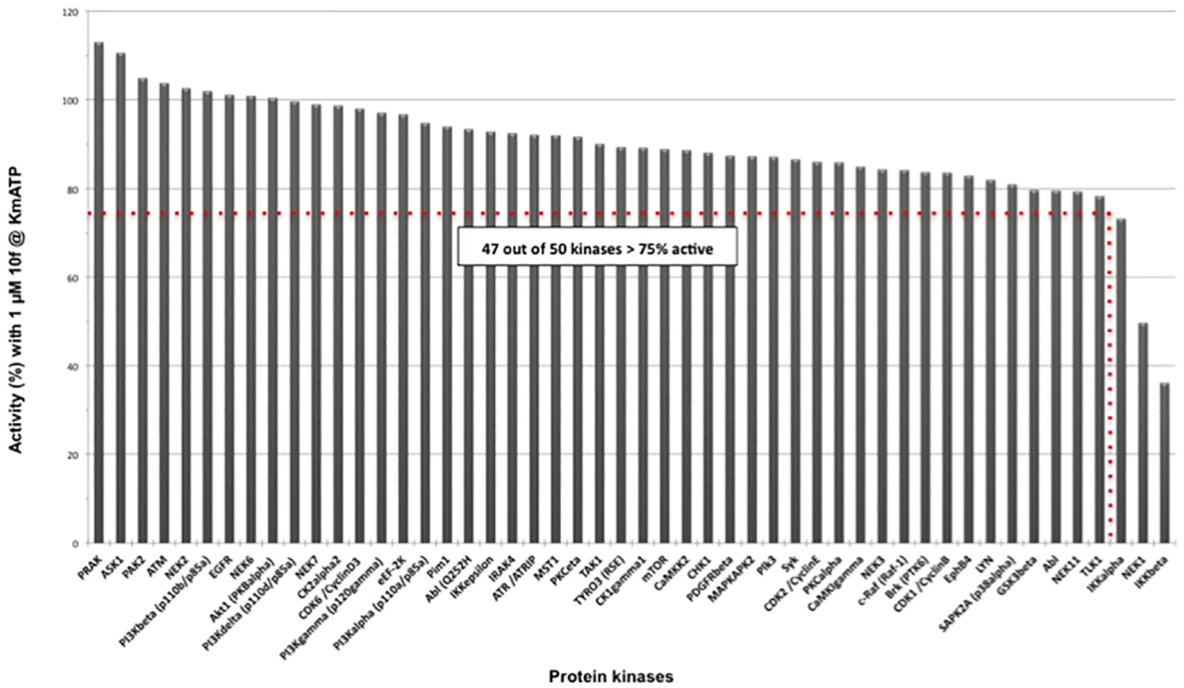

Figure 4. Screening of Compound **10f** against a panel of human protein kinases. Each bar represents the activity of one individual protein kinase. Compound **10f** was tested at a concentration of 1 μM. The ATP concentration was set to the approximate $K_{m,ATP}$ for each kinase tested. See Supporting Information for more details.

which is likely to be substantially disturbed by inhibition and depletion alike.

In order to visualize the influence of **10f** on larval zebrafish nephrogenesis, we implemented a fluorescence-microscopy based imaging pipeline developed by Westhoff et al. (Figure 5).[55] As a means of avoiding dependence on the transgenic *Tg*(*wt1b:EGFP*) zebrafish line, we instead opted for the use of PT-Yellow (BDNCA3-D2), a fluorescent probe that selectively labels the renal proximal tubules in wild-type zebrafish.[56] This approach allowed for zebrafish maintenance and husbandry in a standard laboratory, and it was furthermore reasoned that the ingestion of an external probe is better suited to indicate the impaired renal clearance associated with fluid-filled cysts.[57] As a first step, a bioavailability profile of compound **10f** was evaluated. The aqueous solubility of **10f** in E3-medium (13.9 ± 0.1 μg/mL, Figure S10) was determined in a shake-flask solubility assay, and apical to basolateral transport was determined in a Caco-2 permeability assay (3.4×10^{-6} cm/s, 45% recovery, Table S3). We then determined the minimal lethal concentrations for compound **10f** in a zebrafish developmental toxicity assay over a duration of 120 h. Compound **10f** was added to 6 h postfertilization (hpf) embryos in concentrations ranging from 0.05 μM to 30 μM (Figure S11). Full lethality was only observed close to the solubility limit for a concentration of 30 μM after 72 h. Treatment with **10f** did not induce obvious phenotypes visible to the eye. The treated embryos exhibited normal eye development and body curvature and an ordinary heartbeat.

Based on these results, zebrafish embryos were incubated with (i) the negative control (E3-medium), (ii) 0.2% DMSO, (iii) 10 μM **10f**, and (iv) 20 μM **10f** in E3-medium containing 75 μM 1-phenyl-2-thiourea (PTU) as a melanogenesis inhibitor at 6 hpf. To ensure the stability of **10f** against PTU and PT-Yellow over the duration of the experiment, a stability-indicating HPLC assay was performed in E3-medium (Figure S12). After 48 h, all embryos were treated with 100 nM PT-Yellow for 20 min, thoroughly washed with E3-medium, and returned to the respective compound solution for a total incubation time of 96 h. Finally, the embryos were anesthetized and transferred to agarose molds, which were prepared in 96-well plates according to a published procedure, for fluorescent imaging in a widefield microscope (Figure S13).[55] Administration of **10f** caused a substantial increase in fluorescence intensity (Figure 5D) and expansion (Figure 5E) of the proximal convoluted tubules, thus indicating the growth of fluid-filled cysts, alongside an impaired renal clearance. In addition, our findings provide further evidence for the adequate absorption and bioavailability of **10f**. As hypothesized, our experiments thus demonstrate that Nek1 inhibition by **10f** during early organ development causes cystic kidney growth in zebrafish embryos, despite our findings that **10f** is unselective against IKKβ. Park et al. have shown that levels of phosphorylated-IKKα/β and its downstream factor NF-κB are upregulated in the renal tissue of *PKD2* transgenic mice compared to wild-type controls.[58]

Moreover, Booij et al. demonstrated that cystic growth was in fact reduced by IKKα/β-inhibitors in a murine 3D cell culture based screening platform.[59] It therefore appears that Nek1 inhibition overturns any presumed protective effects of IKKβ inhibition on cystogenesis in our experiments. It should be noted here that, unlike in murine models, zebrafish IKKα is suspected to negatively regulate NF-κB activity. IKK$\alpha^{-/-}$ zebrafish embryos displayed severe head and tail malformations, as well as an upregulated NF-κB response and increased NF-κB-dependent apoptosis, in a study by Correa et al.[60] In accordance with the low IKKα-activity of **10f** (see Table S1), this phenotype was not observed in our experiments. Overall, this leads to the conclusion that the aberrant cystic growth in **10f**-treated zebrafish embryos is unlikely to be mediated by IKK cross-reactivity. However, a causative relation to hitherto

https://dx.doi.org/10.1021/acs.jmedchem.0c02118
J. Med. Chem. XXXX, XXX, XXX−XXX

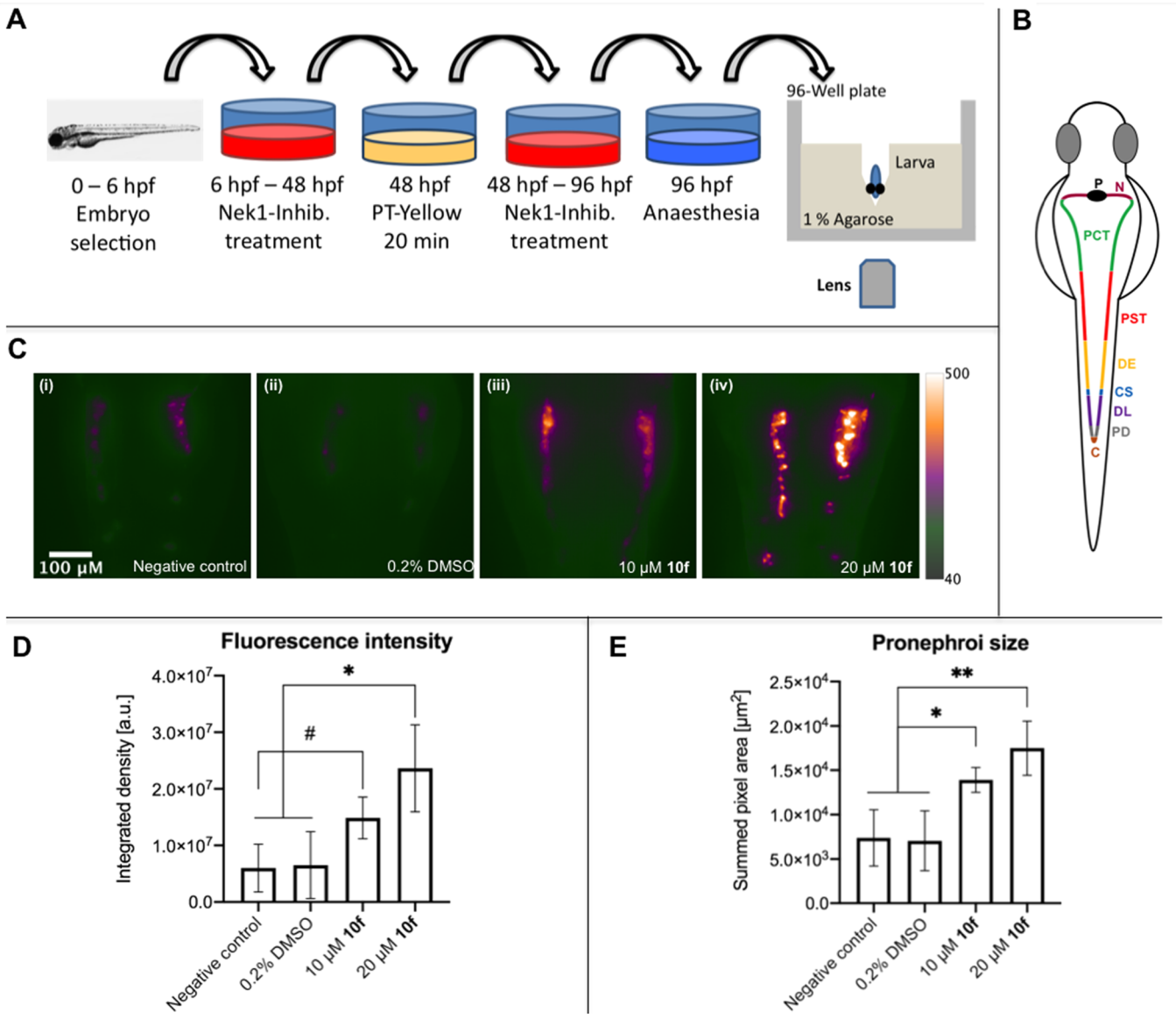

Figure 5. Microscopic imaging of fluorescence-labeled (PT-Yellow) zebrafish pronephroi after treatment with Nek1-inhibitor **10f**. (A) Schematic representation of the workflow, entailing embryo selection, compound treatment, and image acquisition. (B) Schematic representation of the pronephros in the developing zebrafish (28-somite stage). Reprinted with permission from ref 39. Copyright 2018 Gehrig, Pandey and Westhoff. (C) Exemplary maximum intensity projections of deconvolved *Z*-stacks (15× magnification; 33 *Z*-slices; d*Z* = 15 μm). The dotted line indicates the cropped region of interest. (C, i) negative control E3-medium, (C, ii) negative control 0.2% DMSO, (C, iii) 10 μM **10f**, and (C, iv) 20 μM **10f**. (D) Quantification of fluorescence intensity based on summed image projections of deconvolved *Z*-stacks using ImageJ. $n = 3$ for negative control, 0.2% DMSO, and 10 μM **10f**; $n = 5$ for 20 μM **10f** ($^{\#}P = 0.0516$; $^{*}P < 0.05$). (E) Quantification of pronephroi size by summed pixel area determination based on summed image projections of deconvolved *Z*-stacks using ImageJ. $n = 3$ for negative control, 0.2% DMSO, and 10 μM **10f**; $n = 5$ for 20 μM **10f** ($^{*}P < 0.05$; $^{**}P < 0.01$). Abbreviations: au, arbitrary unit; C, Cloaca; CS, corpuscles of Stannius; DE, distal early tubule; DL, distal late tubule; hpf, hours post fertilization; N, neck region; P, podocytes of the glomerulus; PCT, proximal convoluted tubule; PD, pronephric duct; PST, Proximal straight tubule.

unidentified cross-reactivity cannot be ruled out entirely, due to the aforementioned limitations of the selectivity test panel and the fact that the complex PKD-related molecular pathways and regulatory networks are not yet fully understood.[61−63]

CONCLUSION

Based on a published chemical starting point, we generated hypotheses for improved interactions with the Nek1 ATP-binding site by molecular docking into the available crystal structures. These hypotheses were challenged by a series of structurally related inhibitors that were based on the same 4-aryl-7-azaindole scaffold. The most potent compound of this series, **3f**, served as the structural basis of a virtual structure library that encompassed 80 *N*-substituted amino acids and their corresponding alcohols. Seven virtual hits were thereupon identified in an *in silico* virtual library screen in two independent P-loop reconstructed Nek1 3D-structures. This natural product based approach allowed for convenient access to enantiomerically pure starting materials and a straightforward synthetic route and provided the opportunity to exploit nature's own toolkit for protein binding. Our efforts culminated in the ATP-competitive Nek1 inhibitor **10f** that displayed IC_{50} values in the mid to low nanomolar range.

https://dx.doi.org/10.1021/acs.jmedchem.0c02118
J. Med. Chem. XXXX, XXX, XXX−XXX

Moreover, 48 out of 50 kinases were not substantially inhibited by **10f** in a kinase selectivity panel (Figure 4). Ample bioavailability of **10f** was confirmed in a Caco-2 permeability assay, and its toxicity was investigated in wild-type zebrafish embryos. Treatment with **10f** was well tolerated, as full lethality was only observed close to the solubility limit for a concentration of 30 μM. In order to evaluate the *in vivo* efficacy of **10f**, we modified a published procedure for fluorescence microscopy imaging of larval zebrafish pronephroi. As hypothesized, our experiments demonstrated that Nek1 inhibition by **10f** during early organ development causes cystic kidney growth in zebrafish embryos. Our study thus provides the first directed tool compound for a mostly neglected kinase that has been shown to be a key player in numerous forms of cancer and other illnesses, thereby helping to establish Nek1 as a therapeutic target and providing a powerful tool to further elucidate its biological function.

EXPERIMENTAL SECTION

General Information. Unless otherwise noted, starting materials and reagents were purchased from commercial sources and used without further purification. All reactions employing anhydrous conditions were performed in dried glassware with dry solvents under argon atmosphere unless otherwise noted. All cross-coupling reactions were performed with degassed solvents. NMR spectra were recorded on a Bruker Avance II (300 MHz for ^{1}H and 75 MHz for ^{13}C NMR), a Bruker Avance III spectrometer (300 MHz for ^{1}H and 75 MHz for ^{13}C NMR), or a Bruker DRX 500 (500 MHz for ^{1}H and 126 MHz for ^{13}C NMR) spectrometer. Chemical shifts are reported as ppm by frequency downfield of TMS. Coupling constants are reported in Hertz (Hz). Mass spectrometry was performed on a Bruker Daltonik Impact II quadrupol-TOF spectrometer for atmospheric pressure chemical ionization (APCI) and ESI experiments. EI experiments were performed on either a Finnigan MAT95 sector field or a Fisons MD 800 quadrupol spectrometer. HPLC was carried out on an Agilent 1100 system using a Phenomenex Synergi Polar-RP reversed-phase column (4 μm particle size, 150 mm × 3.0 mm, pore size 80 Å) connected to a variable wavelength detector (VWD) or a Phenomenex Synergi Hydro-RP reversed-phase column (4 μm particle size, 150 mm × 3.0 mm, pore size 80 Å) connected to a diode array detector (DAD). Solvent gradient = 30% A for 1 min, linear gradient to 10% A for 10 min, 10% A for 1 min; solvent A = 0.1% TFA in water; solvent B = acetonitrile; flow rate 1.0 mL/min. TLC was performed on precoated 0.2 mm silica gel 60 F254 aluminum sheets (Merck) with detection by UV light (254 and 365 nm) or potassium permanganate staining. Flash chromatography was carried out using the specified solvent systems on 40−63 μm NORMASIL 60 silica gel (VWR). All compounds used in biological or biochemical assays had >95% purity as determined in the HPLC method described above.

General Procedure A: Synthesis of Phenylsulfonamides. Procedure A is exemplified by the triethylamine-mediated sulfonamide formation of compound **2a** from 4-bromobenzenesulfonyl chloride **1** and *N*,*N*-dimethylethylenediamine. Compounds **2b**−**h**, **2j**, **9a**, and **9b** were prepared in accordance with procedure A starting from 4-bromobenzenesulfonyl chloride **1** and the corresponding amine.

General Procedure B: Suzuki−Miyaura Coupling of Aromatic Rings.[40] Procedure B is exemplified by the Suzuki−Miyaura coupling of 4-bromo-7-azaindole and 4-bromo-*N*-(2-(dimethylamino)-ethyl)benzenesulfonamide (**2a**) to give target compound **3a**. Compounds **3b**−**k**, **10a**−**f**, and **7** were prepared in accordance with procedure B starting from 4-bromo-7-azaindole and phenylsulfonamides **2b**−**k** and **9a**−**f** and benzamide **6**, respectively.

4-Bromo-*N*-(2-(dimethylamino)ethyl)benzenesulfonamide (2a). To a stirred solution of 4-bromobenzene-sulfonyl chloride (**1**, 1.00 g, 3.91 mmol) in 10 mL DCM were added *N*,*N*-dimethylethylenediamine (414 mg, 4.70 mmol) and triethylamine (774 mg, 9.78 mmol) at 0 °C under cooling in an ice bath. The cooling bath was removed, and the solution was stirred for 1 h at ambient temperature. The organic layer was washed with water (3 × 5 mL) and brine (5 mL) and dried over $MgSO_4$. The solvent was removed under reduced pressure to give **2a** (1.14 g, 95%) as a light tan solid. ^{1}H NMR ($CDCl_3$, 300 MHz): δ = 7.78−7.71 (m, 2H), 7.69−7.62 (m, 2H), 3.01−2.95 (m, 2H), 2.40−2.33 (m, 2H), 2.11 (s, 6H).

4-Bromo-*N*-(2-(diethylamino)ethyl)benzenesulfonamide (2b). Synthesis of **2b** was performed by following general procedure A using *N*,*N*-dimethylethylenediamine. Yield 74%, yellow oil. ^{1}H NMR ($CDCl_3$, 300 MHz,): δ = 7.77−7.60 (m, 4H), 4.74 (s, 1H), 2.99−2.88 (m, 2H), 2.53−2.45 (m, 2H), 2.39 (q, J = 7.1 Hz, 4H), 0.92 (t, J = 7.1 Hz, 6H). ^{13}C NMR ($CDCl_3$, 75 MHz,): δ = 139.0, 132.4, 128.8, 127.6, 51.1, 46.5, 40.3, 11.7. m/z (EI): 335 ([M]$^+$).

4-Bromo-*N*-(2-(piperidin-1-yl)ethyl)benzenesulfonamide (2c). Synthesis of **2c** was performed by following general procedure A using 1-(2-aminoethyl)piperidine. Yield 91%, orange solid. ^{1}H NMR ($CDCl_3$, 300 MHz): δ = 7.78−7.67 (m, 2H), 7.69−7.58 (m, 2H), 5.31 (s, 1H), 2.95 (dd, J = 6.6, 5.1 Hz, 2H), 2.34 (dd, J = 6.6, 5.1 Hz, 2H), 2.19 (t, J = 5.1 Hz, 4H), 1.43 (dp, J = 22.4, 5.7 Hz, 7H). ^{13}C NMR ($CDCl_3$,75 MHz,) δ = 138.9, 132.4, 128.8, 127.5, 56.2, 54.0, 39.4, 25.9, 24.3. m/z (APCI): 347.05 (M + H)$^+$.

4-Bromo-*N*-(2-morpholinoethyl)benzenesulfonamide (2d). Synthesis of **2d** was performed by following general procedure A using 4-(2-aminoethyl)morpholine. Yield 87%, colorless solid. ^{1}H NMR ($CDCl_3$, 300 MHz): δ = 7.78−7.70 (m, 2H), 7.70−7.62 (m, 2H), 5.29 (s, 1H), 3.67−3.60 (m, 4H), 3.02 (dd, J = 6.7, 4.9 Hz, 2H), 2.46−2.40 (m, 2H), 2.33−2.27 (m, 4H). ^{13}C NMR ($CDCl_3$, 75 MHz): δ = 138.8, 132.4, 128.6, 127.6, 66.7, 56.3, 53.0, 38.9. m/z (APCI): 349.03 (M + H)$^+$.

***tert*-Butyl (2-(4-Bromophenyl)sulfonamido)ethyl)-carbamate (2e).** Synthesis of **2e** was performed by following general procedure A using *N*-Boc-ethylenediamine. Yield 78%, colorless solid. ^{1}H NMR ($CDCl_3$, 300 MHz): δ = 7.76−7.59 (m, 4H), 5.05 (s, 1H), 3.24−3.18 (m, 2H), 3.04 (dd, J = 6.3, 4.8 Hz, 2H), 1.41 (s, 9H). ^{13}C NMR ($CDCl_3$, 75 MHz,): δ = 156.8, 139.2, 132.5, 128.7, 127.6, 52.6, 46.3, 43.9, 42.0, 40.4, 28.54, 28.47, 10.7. m/z (EI): 380 ([M$^+$]).

4-Bromo-*N*-(2-hydroxyethyl)benzenesulfonamide (2f). Synthesis of **2f** was performed by following general procedure A using 2-aminoethanol. Yield 81%, colorless solid. ^{1}H NMR (DMSO-*d*6, 300 MHz): δ = 7.84−7.70 (m, 4H), 4.67 (t, J = 5.5 Hz, 1H), 3.40−3.32 (m, 2H), 2.80 (q, J = 6.1 Hz, 2H). m/z (APCI): 279.96 ([M + H]$^+$).

4-Bromo-*N*-(2-methoxyethyl)benzenesulfonamide (2g). Synthesis of **2g** was performed by following general procedure A using 2-methoxyethylamine. Yield 78%, yellow oil. ^{1}H NMR (DMSO-d_6, 300 MHz,): δ = 7.82−7.78 (m, 2H), 7.75−7.69 (m, 2H), 3.32 (s, 3H), 3.29 (t, J = 5.6 Hz, 2H), 2.92 (q, J = 5.8 Hz, 2H).

4-Bromo-*N*-(2-hydroxyethyl)-*N*-methylbenzenesulfonamide (2h). Synthesis of **2h** was performed by following general procedure A using *N*-methylethanolamine. Yield 90%, colorless oil. ^{1}H NMR ($CDCl_3$, 300 MHz): δ = 7.68 (s, 4H), 3.78 (dd, J = 5.6, 4.9 Hz, 2H), 3.18 (t, J = 5.3 Hz, 2H), 2.85 (s, 3H). m/z (APCI): 293.98 ([M + H]$^+$).

2-((4-Bromophenyl)sulfonamido)ethyl acetate (2i). To a stirred solution of **2f** (0.77 g, 2.73 mmol) and triethylamine (0.33 g, 3.28 mmol) in 5 mL of DCM, acetanhydride (0.34 g, 3.28 mmol) was added dropwise at 0 °C under cooling in an ice bath. The cooling bath was removed, and the solution was stirred for 72 h at ambient temperature. The reaction mixture was diluted with 20 mL of DCM and quenched by bringing the pH to 9 through addition of saturated $NaHCO_3$ (aq). The organic layer was washed with saturated $NaHCO_3$ (aq, 3 × 5 mL) and brine (5 mL) and dried over $MgSO_4$. The solvent was removed under reduced pressure to give **2i** (0.73 g, 82%) as a yellow oil that was used without further purification. ^{1}H NMR (DMSO-d_6, 300 MHz): δ = 7.85−7.80 (m, 2H), 7.75−7.69 (m, 2H), 3.95 (t, J = 5.6 Hz, 2H), 3.03 (q, J = 5.6 Hz, 2H), 1.93 (s, 3H). m/z (ESI): 343.96 ([M + Na]$^+$).

https://dx.doi.org/10.1021/acs.jmedchem.0c02118
J. Med. Chem. XXXX, XXX, XXX−XXX

4-Bromo-*N*-(2-hydroxy-2-methylpropyl)-benzenesulfonamide (2j). Synthesis of **2j** was performed by following general procedure A using 1-amino-2-methyl-2-propanol. Yield 64%, yellow solid. ^{1}H NMR (DMSO-d_6, 500 MHz): δ = 7.83−7.78 (m, 2H), 7.75−7.71 (m, 2H), 7.59 (t, J = 6.5 Hz, 1H), 4.40 (s, 1H), 2.62 (d, J = 6.5 Hz, 2H), 1.04 (s, 6H). ^{13}C NMR (DMSO-d_6, 126 MHz): δ = 140.1, 132.1, 128.5, 125.9, 68.7, 53.6, 27.0. ^{13}C NMR (DMSO-d_6, 126 MHz, DEPT): δ = 132.1, 128.6, 53.6, 45.5, 27.1, 8.5. m/z (APCI): 307.98 ([M + H]$^+$).

1-((4-Bromophenyl)sulfonyl)-4-methylpiperazine (2k). To a solution of 4-bromobenzene-sulfonyl chloride (0.40 g, 1.47 mmol) in 9 mL of dry THF, 1-methyl-piperazine (1.41 g, 14.09 mmol) was added, and the mixture was stirred for 16 h at ambient temperature. The solvent was removed under reduced pressure, and the resulting residue was dissolved in 10 mL of DCM. The organic layer was washed with saturated $NaHCO_3$ (aq, 3 × 2.5 mL) and dried over $MgSO_4$. The solvent was removed under reduced pressure to give **2k** (0.37 g, 75%) as a yellow solid. ^{1}H NMR ($CDCl_3$, 500 MHz): δ = 7.69−7.63 (m, 2H), 7.62−7.58 (m, 2H), 3.03 (t, J = 4.9 Hz, 4H), 2.47 (t, J = 5.0 Hz, 4H), 2.26 (s, 3H). ^{13}C NMR ($CDCl_3$,126 MHz): δ = 134.7, 132.4, 129.4, 128.0, 54.1, 46.0, 45.8. m/z (EI): 380 ([M]$^+$).

((4-Bromophenyl)sulfonyl)-L-phenylalanine (2l). To a stirred solution of L-phenylalanine (194 mg, 1.17 mmol) in 4 mL of water was added sodium bicarbonate (296 mg, 3.52 mmol). The mixture was stirred at ambient temperature for 15 min, and a solution of 4-bromobenzenesulfonyl chloride (**1**, 300 mg, 1.17 mmol) in 4 mL of acetone was added at 0 °C under cooling in an ice bath. The cooling bath was removed, and the solution was stirred at ambient temperature for 20 h. After evaporation of the volatile solvent under reduced pressure, the product was precipitated by bringing the pH to 7 using hydrochloric acid (1 N). Filtration and drying under reduced pressure gave **2l** (220 mg, 49%) as a yellow solid. ^{1}H NMR (DMSO-d_6, 500 MHz): δ = 7.72−7.69 (m, 2H), 7.65−7.61 (m, 2H), 7.18−7.11 (m, 5H), 3.35 (t, J = 5.1 Hz, 1H), 2.98 (dd, J = 13.4, 5.0 Hz, 1H), 2.90 (dd, J = 13.4, 5.2 Hz, 1H). ^{13}C NMR (DMSO-d_6, 126 MHz): δ = 170.8, 139.7, 138.7, 132.0, 129.9, 128.7, 127.5, 125.9, 125.6, 58.3, 38.5. m/z (ESI): 788.95 ([2M + Na]$^+$), 405.97 ([M + Na]$^+$), 383.99 ([M + H]$^+$).

***N*-(2-(Dimethylamino)ethyl)-4-(1*H*-pyrrolo[2,3-*b*]pyridin-4-yl)benzenesulfonamide (3a).** To a solution of sulfonamide **2a** (100 mg, 0.33 mmol) in 1.5 mL of DMF were added potassium acetate (97 mg, 0.99 mmol), bis(pinacolato)diboron (100 mg, 0.40 mmol), and $PdCl_2$(dppf) (7 mg, 10 μmol), under argon atmosphere. The reaction mixture was stirred at 100 °C for 3 h. After cooling to ambient temperature, 15 mL of ethyl acetate was added, the solution was filtered through Celite, and the organic layer was washed with brine (5 × 15 mL) before drying over $NaSO_4$. The solvent was removed under reduced pressure to give the corresponding boronic acid pinacolester as a crude solid that was dissolved in 1.5 mL of DMF and treated with 4-bromo-7-azaindole (65 mg, 0.33 mmol), 0.5 mL of saturated $NaHCO_3$ (aq) and $Pd(PPh_3)_4$ (38 mg, 36 μmol) under argon atmosphere. The mixture was stirred at 100 °C for 18 h, cooled to ambient temperature, and diluted with 20 mL of EtOAc. After filtration through Celite, the organic layer was washed with brine (5 × 20 mL) and dried over $MgSO_4$, and the solvent was removed under reduced pressure. Purification was performed by column chromatography using a 10:1:0.1 mixture of DCM/MeOH/NH_3 in MeOH (7 N) to give **3a** (47 mg, 42%) as a colorless solid. ^{1}H NMR (DMSO-d_6, 300 MHz): δ = 11.89 (s, 1H), 8.33 (d, J = 4.9 Hz, 1H), 7.98 (s, 4H), 7.60 (d, J = 3.5 Hz, 1H), 7.25 (d, J = 4.9 Hz, 1H), 6.64 (d, J = 3.5 Hz, 1H), 2.91 (t, J = 6.8 Hz, 2H), 2.28 (t, J = 6.8 Hz, 2H), 2.07 (s, 6H). ^{13}C NMR (DMSO-d_6, 75 MHz,): δ = 149.2, 142.9, 142.2, 140.3, 138.5, 128.9, 127.2, 127.2, 117.1, 114.4, 98.8, 58.1, 45.0, 40.7. m/z (APCI): 345.13 ([M + H]$^+$).

***N*-(2-(Diethylamino)ethyl)-4-(1*H*-pyrrolo[2,3-*b*]pyridin-4-yl)-benzenesulfonamide (3b).** Starting from **2b**, the synthesis of **3b** was performed by following general procedure B. Purification was performed by column chromatography using a 10:1:0.1 mixture of DCM/MeOH/NH_3 in MeOH (7 N). Yield 41%, beige semisolid. ^{1}H NMR (DMSO-d_6, 500 MHz): δ = 11.88 (s, 1H), 8.33 (d, J = 4.9 Hz, 1H), 8.04−7.90 (m, 4H), 7.60 (d, J = 3.5 Hz, 1H), 7.25 (d, J = 4.9 Hz, 1H), 6.63 (d, J = 3.5 Hz, 1H), 2.88 (dd, J = 8.1, 6.3 Hz, 2H), 2.43 (t, J = 7.2 Hz, 2H), 2.39 (q, J = 7.1 Hz, 4H), 0.86 (t, J = 7.1 Hz, 6H). ^{13}C NMR (DMSO-d_6, 126 MHz): δ = 149.2, 142.9, 142.2, 140.3, 138.5, 128.9, 127.2, 127.1, 117.1, 114.3, 98.7, 51.8, 46.5, 41.0, 11.6. ^{13}C NMR (126 MHz, DMSO-d_6, DEPT) δ = 142.9, 128.9, 127.1, 114.36, 98.7, 51.8, 46.5, 41.0, 11.6. m/z (ESI): 373.18 ([M + H]$^+$), 187.09 ([M + 2H]$^{2+}$). Mp: 143 °C.

***N*-(2-(Piperidin-1-yl)ethyl)-4-(1*H*-pyrrolo[2,3-*b*]pyridin-4-yl)-benzenesulfonamide (3c).** Starting from **2c**, the synthesis of **3c** was performed by following general procedure B. Purification was performed by column chromatography using a 15:1:0.1 mixture of DCM/MeOH/NH_3 in MeOH (7 N). Yield 58%, beige solid. ^{1}H NMR (DMSO-d_6, 300 MHz): δ = 11.88 (s, 1H), 8.32 (d, J = 4.8 Hz, 1H), 7.97 (s, 4H), 7.60 (d, J = 3.4 Hz, 1H), 7.25 (d, J = 4.8 Hz, 1H), 6.63 (d, J = 3.4 Hz, 1H), 2.92 (t, J = 6.9 Hz, 2H), 2.29 (t, J = 6.9 Hz, 2H), 2.23 (t, J = 5.0 Hz, 4H), 1.45−1.21 (m, 6H). ^{13}C NMR (DMSO-d_6, 75 MHz,): δ = 149.2, 142.9, 142.1, 140.3, 138.5, 128.9, 127.2, 127.1, 117.1, 114.4, 98.7, 57.6, 53.9, 40.3, 25.4, 23.9. ^{13}C NMR (DMSO-d_6, 75 MHz, DEPT): δ = 142.9, 128.9, 127.2, 127.1, 114.4, 98.7, 57.6, 53.9, 40.2, 25.34, 23.9. m/z (APCI): 385.18 ([M + H]$^+$). Mp: 204 °C.

***N*-(2-Morpholinoethyl)-4-(1*H*-pyrrolo[2,3-*b*]pyridin-4-yl)-benzenesulfonamide (3d).** Starting from **2d**, the synthesis of **3d** was performed by following general procedure B. Purification was performed by column chromatography using a 50:1:0.5 mixture of DCM/MeOH/NH_3 in MeOH (7 N). Yield 69%, beige solid. ^{1}H NMR (DMSO-d_6, 500 MHz,): δ = 11.88 (s, 1H), 8.33 (d, J = 4.9 Hz, 1H), 7.98 (s, 4H), 7.65 (t, J = 5.9 Hz, 1H), 7.60 (dd, J = 3.5, 2.5 Hz, 1H), 7.25 (d, J = 4.9 Hz, 1H), 6.64 (dd, J = 3.5, 1.8 Hz, 1H), 3.52−3.46 (m, 4H), 2.95 (q, J = 6.3 Hz, 2H), 2.33 (t, J = 6.8 Hz, 2H), 2.27 (t, J = 4.7 Hz, 4H). ^{13}C NMR (DMSO-d_6, 126 MHz) δ = 149.2, 142.9, 142.1, 140.3, 138.46, 128.9, 127.2, 127.1, 117.1, 114.4, 98.7, 66.0, 57.2, 53.1, 39.9. ^{13}C NMR (DMSO-d_6, 126 MHz, DEPT) δ = 142.9, 128.9, 127.2, 127.1, 114.4, 98.7, 66.0, 57.2, 53.1, 39.8. m/z (APCI): 387.16 ([M + H]$^+$). Mp: 201 °C.

***tert*-Butyl(2-((4-(1*H*-pyrrolo[2,3-*b*]pyridin-4-yl)phenyl)-sulfonamido)ethyl)carbamate (3e).** Starting from **2e**, the synthesis of **3e** was performed by following general procedure B. Purification was performed by column chromatography using a 20:1:0.1 mixture of DCM/MeOH/NH_3 in MeOH (7 N). Yield 60%, colorless solid. ^{1}H NMR (DMSO-d_6,500 MHz,): δ = 11.88 (s, 1H), 8.33 (d, J = 4.9 Hz, 1H), 8.01−7.93 (m, 4H), 7.76 (t, J = 6.0 Hz, 1H), 7.60 (dd, J = 3.5, 2.6 Hz, 1H), 7.26 (d, J = 4.9 Hz, 1H), 6.78 (t, J = 5.9 Hz, 1H), 6.66 (dd, J = 3.5, 1.8 Hz, 1H), 3.01 (q, J = 6.6 Hz, 2H), 2.84 (q, J = 6.4 Hz, 2H), 1.34 (s, 9H). ^{13}C NMR (DMSO-d_6, 126 MHz): δ = 155.5, 149.2, 142.9, 142.2, 140.0, 138.4, 129.0, 127.2, 127.1, 117.1, 114.4, 98.8, 77.8, 42.3, 28.1. ^{13}C NMR (DMSO-d_6, 126 MHz, DEPT): δ = 142.9, 129.0, 127.2, 127.1, 114.4, 98.8, 42.3, 39.8, 28.2. m/z (APCI): 417.16 ([M + H]$^+$).

***N*-(2-Hydroxyethyl)-4-(1*H*-pyrrolo[2,3-*b*]pyridin-4-yl)benzenesulfonamide (3f).** Starting from **2f**, the synthesis of **3f** was performed by following general procedure B. Purification was performed by column chromatography using a 10:1:0.1 mixture of DCM/MeOH/NH_3 in MeOH (7 N). Yield 66%, colorless solid. ^{1}H NMR (DMSO-d_6, 500 MHz): δ = 11.88 (s, 1H), 8.33 (d, J = 4.9 Hz, 1H), 8.01−7.94 (m, 4H), 7.71 (t, J = 5.9 Hz, 1H), 7.60 (t, J = 3.0 Hz, 1H), 7.26 (d, J = 5.0 Hz, 1H), 6.65 (dd, J = 3.5, 1.8 Hz, 1H), 4.70 (t, J = 5.6 Hz, 1H), 3.42 (q, J = 6.0 Hz, 2H), 2.88 (q, J = 6.2 Hz, 2H). ^{13}C NMR (DMSO-d_6, 126 MHz): δ = 149.2, 142.9, 142.1, 140.2, 138.5, 128.9, 127.2, 127.12, 117.1, 114.4, 98.8, 59.9, 45.1. ^{13}C NMR (DMSO-d_6, 126 MHz, DEPT): δ = 142.9, 128.9, 127.2, 127.1, 114.4, 98.8, 60.0, 45.1. m/z (ESI): 318.09 ([M + H]$^+$).

***N*-(2-Methoxyethyl)-4-(1*H*-pyrrolo[2,3-*b*]pyridin-4-yl)-benzenesulfonamide (3g).** Starting from **2g**, the synthesis of **3g** was performed by following general procedure B. Purification was performed by column chromatography using a 20:1:0.1 mixture of DCM/MeOH/NH_3 in MeOH (7 N). Yield 65%, colorless solid. ^{1}H NMR (DMSO-d_6, 500 MHz): δ = 11.88 (s, 1H), 8.33 (d, J = 4.9 Hz, 1H), 8.02−7.91 (m, 4H), 7.83 (t, J = 6.0 Hz, 1H), 7.60 (dd, J = 3.5,

https://dx.doi.org/10.1021/acs.jmedchem.0c02118
J. Med. Chem. XXXX, XXX, XXX−XXX

2.5 Hz, 1H), 7.25 (d, J = 4.9 Hz, 1H), 6.65 (dd, J = 3.6, 1.8 Hz, 1H), 3.34 (t, J = 5.7 Hz, 2H), 2.99 (q, J = 5.8 Hz, 2H). ^{13}C NMR (DMSO-d_6, 126 MHz): δ = 149.17, 142.92, 142.15, 140.35, 138.49, 128.87, 127.19, 127.10, 117.13, 114.38, 98.76, 70.56, 57.83, 42.24. ^{13}C NMR (DMSO-d_6, 126 MHz, DEPT): δ = 142.92, 128.87, 127.19, 127.10, 114.38, 98.76, 70.56, 57.83, 42.24. m/z (APCI): 332.10 ([M + H]$^+$). Mp: 215 °C.

***N*-(2-Hydroxyethyl)-*N*-methyl-4-(1*H*-pyrrolo[2,3-*b*]pyridin-4-yl)benzenesulfonamide (3h).** Starting from **2h**, the synthesis of **3h** was performed by following general procedure B. Purification was performed by column chromatography using a 20:1:0.1 mixture of DCM/MeOH/NH_3 in MeOH (7 N). Yield 42%, colorless solid. ^{1}H NMR (DMSO-d_6, 500 MHz): δ = 11.89 (s, 1H), 8.33 (d, J = 4.9 Hz, 1H), 8.01 (d, J = 8.4 Hz, 2H), 7.93 (d, J = 8.4 Hz, 2H), 7.60 (t, J = 3.0 Hz, 1H), 7.27 (d, J = 5.0 Hz, 1H), 6.66 (dd, J = 3.6, 1.8 Hz, 1H), 4.81 (td, J = 5.5, 1.3 Hz, 1H), 3.56 (q, J = 5.8 Hz, 2H), 3.10 (t, J = 6.1 Hz, 2H), 2.80 (s, 3H). ^{13}C NMR (DMSO-d_6, 126 MHz): δ = 149.2, 142.9, 142.6, 138.25, 136.82, 129.03, 127.71, 127.24, 117.07, 114.36, 98.7, 59.1, 51.94 35.6. ^{13}C NMR (DMSO-d_6, 126 MHz, DEPT): δ = 142.9, 142.7, 129.0, 127.7, 127.2, 114.4, 98.7, 59.1, 51.94, 35.6. m/z (APCI): 332.11 ([M + H]$^+$).

2-((4-(1*H*-Pyrrolo[2,3-*b*]pyridin-4-yl)phenyl)sulfonamido)-ethyl Acetate (3i). Starting from **2i**, the synthesis of **3i** was performed by following general procedure B. Purification was performed by column chromatography using a 15:1:0.1 mixture of DCM/MeOH/NH_3 in MeOH (7 N). Yield 23%, colorless solid. ^{1}H NMR (DMSO-d_6, 500 MHz): δ = 11.90 (s, 1H), 8.35 (d, J = 5.0 Hz, 1H), 8.03−7.96 (m, 5H), 7.62 (dd, J = 3.5, 2.5 Hz, 1H), 7.28 (d, J = 5.0 Hz, 1H), 6.67 (dd, J = 3.5, 1.9 Hz, 1H), 4.02 (t, J = 5.6 Hz, 2H), 3.12 (q, J = 5.7 Hz, 2H), 1.96 (s, 3H). ^{13}C NMR (DMSO-d_6, 126 MHz): δ = 170.2, 149.18, 142.94, 142.28, 140.22, 138.45, 128.98, 127.23, 127.1, 117.1, 114.4, 98.8, 62.5, 41.4, 20.6. m/z (APCI): 360.10 ([M + H]$^+$).

***N*-(2-Hydroxy-2-methylpropyl)-4-(1*H*-pyrrolo[2,3-*b*]pyridin-4-yl)benzenesulfonamide (3j).** Starting from **2j**, the synthesis of **3j** was performed by following general procedure B. Purification was performed by column chromatography using a 13:1:0.1 mixture of DCM/MeOH/NH_3 in MeOH (7 N). Yield 11%, colorless solid. ^{1}H NMR (DMSO-d_6, 500 MHz): δ = 11.87 (s, 1H), 8.33 (d, J = 4.9 Hz, 1H), 8.01−7.94 (m, 4H), 7.62−7.54 (m, 2H), 7.26 (d, J = 4.9 Hz, 1H), 6.65 (dd, J = 3.5, 1.9 Hz, 1H), 4.42 (s, 1H), 2.70 (d, J = 6.6 Hz, 2H), 1.08 (s, 6H). ^{13}C NMR (DMSO-d_6, 126 MHz): δ = 149.2, 142.9, 142.1, 140.4, 138.5, 128.9, 127.18, 127.16, 117.1, 114.4, 98.8, 68.8, 53.7, 27.1. ^{13}C NMR (DMSO-d_6, 126 MHz, DEPT): δ = 142.9, 128.9, 127.18, 127.16, 114.4, 98.8, 53.7, 27.1. m/z (EI): 345 ([M]$^+$).

4-(4-((4-Methylpiperazin-1-yl)sulfonyl)phenyl)-1*H*-pyrrolo-[2,3-*b*]pyridine (3k). Starting from **2k**, the synthesis of **3k** was performed by following general procedure B. Purification was performed by column chromatography using a 20:1:0.1 mixture of DCM/MeOH/NH_3 in MeOH (7 N). Yield 58%, colorless solid. ^{1}H NMR (D_2O, as a TFA salt, 500 MHz): δ = 8.39 (d, J = 6.0 Hz, 1H), 8.00−7.87 (m, 4H), 7.72 (d, J = 3.6 Hz, 1H), 7.54 (d, J = 6.0 Hz, 1H), 6.82 (d, J = 3.6 Hz, 1H), 4.02 (d, J = 13.5 Hz, 2H), 3.68 (d, J = 12.7 Hz, 2H), 3.33 (td, J = 12.5, 3.3 Hz, 2H), 2.98 (s, 3H), 2.95−2.86 (m, 2H). ^{13}C NMR (D_2O, as a TFA salt, 126 MHz,): δ = 146.8, 141.2, 139.6, 135.1, 133.6, 130.2, 130.0, 128.1, 122.9, 114.9, 101.7, 52.7, 43.2, 42.8. ^{13}C NMR (D_2O, as a TFA salt, 126 MHz, DEPT): δ = 133.5, 130.2, 130.0, 128.1, 114.9, 101.7, 52.7, 43.3, 42.8. m/z (APCI): 357.15 ([M + H]$^+$).

((4-(1*H*-Pyrrolo[2,3-*b*]pyridin-4-yl)phenyl)sulfonyl)-L-phenylalanine (3l). To a solution of sulfonamide **2l** (200 mg, 0.52 mmol) in 3 mL of DMF were added potassium acetate (153 mg, 1.56 mmol), bis(pinacolato)diboron (159 mg, 0.62 mmol), and $PdCl_2$(dppf) (13 mg, 15 μmol) under argon atmosphere. The reaction mixture was stirred at 100 °C for 3 h. After cooling to ambient temperature 20 mL of EtOAc was added, the solution was filtered through Celite, and the organic layer was washed with brine (5 × 20 mL) before drying over $NaSO_4$. The solvent was removed under reduced pressure to give the corresponding boronic acid pinacolester as a crude solid that was dissolved in 3 mL of DMF and treated with 4-bromo-7-azaindole (103 mg, 0.52 mmol), 1 mL of saturated $NaHCO_3$ (aq), and $Pd(PPh_3)_4$ (60 mg, 52 μmol) under argon atmosphere. The mixture was stirred at 100 °C for 17 h, cooled to ambient temperature, and diluted with 20 mL of EtOAc. After filtration through Celite, the organic layer was washed with brine (5 × 20 mL), and the product was precipitated by setting the pH to 4 using hydrochloric acid (0.1 N). Filtration and drying under reduced pressure gave **3l** (55 mg, 25%) as a colorless solid. ^{1}H NMR (DMSO-d_6, 500 MHz): δ = 11.89 (s, 1H), 8.41 (d, J = 9.0 Hz, 1H), 8.33 (d, J = 4.9 Hz, 1H), 7.80 (d, J = 8.1 Hz, 2H), 7.70 (d, J = 8.3 Hz, 2H), 7.61 (t, J = 3.0 Hz, 1H), 7.22 (d, J = 4.9 Hz, 1H), 7.20−7.10 (m, 5H), 6.62 (dd, J = 3.5, 1.7 Hz, 1H), 3.95 (dt, J = 8.8, 4.0 Hz, 1H), 2.99 (dd, J = 13.8, 5.5 Hz, 1H), 2.79−2.72 (m, 1H). ^{13}C NMR (DMSO-d_6, 126 MHz): δ = 172.4, 149.2, 142.9, 141.9, 140.6, 138.6, 136.8, 129.1, 128.5, 128.1, 127.2, 126.8, 126.4, 117.1, 114.3, 98.8, 57.5, 57.5, 37.8. m/z (APCI): 422.12 ([M + H]$^+$).

2-(4-Bromobenzamido)ethyl 4-Bromobenzoate (5). A solution of 4-bromobenzoyl chloride (**4**, 2.00 g, 9.11 mmol) in 10 mL of DCM was dropwise added to a solution of monoethanolamine (0.67 g, 10.94 mmol) and triethylamine (1.08 g, 6.78 mmol) in 10 mL of DCM over the course of 20 min. The mixture was stirred at ambient temperature for 24 h, diluted with 10 mL DCM, and washed with saturated $NaHCO_3$ (aq, 3 × 5 mL). The organic layer was dried over $MgSO_4$, and the solvent was removed to give a colorless residue that was recrystallized from EtOH to give **5** (0.60 g, 48%) as a colorless solid. ^{1}H NMR (DMSO-d_6, 500 MHz): δ = 8.76 (t, J = 5.6 Hz, 1H), 7.92−7.87 (m, 2H), 7.81−7.76 (m, 2H), 7.75−7.70 (m, 2H), 7.70−7.64 (m, 2H), 4.40 (t, J = 5.5 Hz, 2H), 3.64 (q, J = 5.6 Hz, 2H). ^{13}C NMR (DMSO-d_6, 126 MHz): δ = 165.7, 165.1, 133.4, 131.8, 131.3, 131.2, 129.3, 128.9, 127.3, 124.9, 63.6, 38.4. ^{13}C NMR (DMSO-d_6, 126 MHz, DEPT): δ = 131.8, 131.3, 131.2, 129.3, 63.6, 38.4. m/z (ESI): 425.93 ([M + H]$^+$).

4-Bromo-*N*-(2-hydroxyethyl)benzamide (6). To a solution of ester **5** (0.50 g, 1.17 mmol) in 20 mL of THF was added 2 mL of 50% w/v aq. KOH solution, and the mixture was stirred at 60 °C for 16 h. The solvent was removed under reduced pressure, and the resulting white residue was taken up in 20 mL of EtOAc and washed with water (3 × 5 mL) and brine (5 mL). Purification was performed by column chromatography using a 15:1 mixture of DCM/MeOH to give **6** (262 mg, 92%) as a colorless solid. ^{1}H NMR (DMSO-d_6, 500 MHz): δ = 8.49 (t, J = 5.7 Hz, 1H), 7.82−7.77 (m, 2H), 7.68−7.65 (m, 2H), 4.70 (t, J = 5.6 Hz, 1H), 3.51 (q, J = 5.9 Hz, 2H), 3.32 (q, J = 6.1 Hz, 2H). ^{13}C NMR (DMSO-d_6, 126 MHz): δ = 165.4, 133.7, 131.2, 129.3, 124.73, 59.6, 42.2. m/z (EI): 243 ([M]$^+$).

***N*-(2-Hydroxyethyl)-4-(1*H*-pyrrolo[2,3-*b*]pyridin-4-yl)-benzamide (7).** Starting from **6**, the synthesis of 7 was performed by following general procedure B. Purification was performed by column chromatography using a stepwise gradient from a 15:1:0.1 to a 10:1:0.1 mixture of DCM/MeOH/10% aq. NH_4OH (25%) in MeOH. Yield 43%, colorless solid. ^{1}H NMR (DMSO-d_6, 500 MHz): δ = 11.83 (s, 1H), 8.53 (t, J = 5.6 Hz, 1H), 8.31 (d, J = 4.9 Hz, 1H), 8.07−8.00 (m, 2H), 7.89−7.82 (m, 2H), 7.60−7.55 (m, 1H), 7.23 (d, J = 4.9 Hz, 1H), 6.63 (dd, J = 3.6, 1.8 Hz, 1H), 4.75 (t, J = 5.6 Hz, 1H), 3.56 (q, J = 6.0 Hz, 2H), 3.39 (q, J = 6.1 Hz, 2H). ^{13}C NMR (DMSO-d_6, 126 MHz): δ = 165.9, 149.2, 142.9, 141.0, 139.3, 134.2, 128.0, 127.8, 126.9, 117.2, 114.3, 99.0, 59.8, 42.2. ^{13}C NMR (DMSO-d_6, 126 MHz, DEPT): δ = 142.9, 128.0, 127.9, 126.9, 114.3, 98.9, 59.8, 42.3. m/z (ESI): 282.12 ([M + H]$^+$).

(*R*)-4-(2-Amino-3-hydroxypropyl)phenol (8d). To a stirred solution of D-tyrosine methyl ester hydrochloride (2.00 g, 8.63 mmol) in 20 mL of acetonitrile was added potassium carbonate (2.98 g, 21.6 mmol), and the solution was heated to 50 °C for 16 h. Filtration of the formed salt and evaporation of the solvent under reduced pressure gave an orange oil that was taken up in 20 mL of methanol. Under cooling to 0 °C in an ice bath, $NaBH_4$ (491 mg, 12.99 mmol) was added in small portions over 30 min. The cooling bath was removed, and the solution was stirred at ambient temperature for 5 h. The solvent was removed under reduced pressure, the resulting residue was taken up in 50 mL of water, and the aqueous layer was extracted with ethyl acetate (5 × 50 mL). The combined organic layers were

https://dx.doi.org/10.1021/acs.jmedchem.0c02118
J. Med. Chem. XXXX, XXX, XXX−XXX

dried over $MgSO_4$, filtered, and concentrated *in vacuo* to give **8d** (878 mg, 61%) as a crude yellow solid that was used for the next step without further purification. ^{1}H NMR (DMSO-d_6, 500 MHz): δ = 6.68−6.65 (m, 2H), 6.37−6.34 (m, 2H), 2.97 (dd, J = 10.3, 4.5 Hz, 1H), 2.87−2.83 (m, 1H), 2.24 (dd, J = 13.4, 6.0 Hz, 1H), 2.20−2.09 (m, 1H), 2.02 (dd, J = 13.4, 7.5 Hz, 1H), 1.44 (s, 1H). ^{13}C NMR (DMSO-d_6, 500 MHz): δ = 155.5, 130.0, 129.5, 115.0, 65.5, 54.6, 39.0. m/z (EI): 167 ([M]$^+$).

(*S*)-2-Amino-3-(1*H*-indol-3-yl)propan-1-ol (8e). An oven-dried three-neck flask was charged with L-tryptophan (2.04 g, 10.0 mmol), sodium borohydride (757 mg, 20.0 mmol), and 20 mL of dry THF and equipped with a dropping funnel and a reflux condenser under argon atmosphere. A solution of iodine (2.54 g, 10.0 mmol) in 10 mL dry THF was added dropwise over the course of 30 min at 0 °C under cooling in an ice bath. Once the evolution of gas had stopped, the ice bath was removed, and the mixture was heated to reflux for 20 h. After cooling to ambient temperature, methanol was slowly added under vigorous stirring until the solution became clear. After stirring for another 15 min, removal of the solvents under reduced pressure gave a white residue that was dissolved in 25 mL of aq. KOH solution (20% w/v) and stirred for 16 h at ambient temperature. Adjustment to pH 11 by addition of hydrochloric acid (2 M) was followed by extraction of the aqueous layer with DCM (3 × 25 mL) and a 1:4 mixture of ethanol/chloroform (5 × 25 mL). The combined organic layers were washed with water (3 × 25 mL) and brine (25 mL) and dried over $MgSO_4$. The solvent was removed under reduced pressure to give **8e** (1.36 g, 72%) as a crude yellow oil that was used without further purification. ^{13}C NMR (75 MHz, $CDCl_3$) δ = 136.5, 127.7, 122.9, 122.1, 119.4, 118.9, 112.4, 111.4, 66.6, 53.1, 30.1. m/z (ESI): 191.12 ([M + H]$^+$).

(*R*)-2-Amino-3-(1*H*-indol-3-yl)propan-1-ol (8f). An oven-dried three-neck flask was charged with D-tryptophan (1.57 g, 7.69 mmol), sodium borohydride (640 mg, 16.91 mmol), and 15 mL of dry THF and equipped with a dropping funnel and a reflux condenser under argon atmosphere. A solution of iodine (1.95 g, 7.69 mmol) in 8 mL of dry THF was added dropwise over the course of 30 min at 0 °C under cooling in an ice bath. Once the evolution of gas had stopped, the ice bath was removed, and the mixture was heated to reflux for 19 h. After the mixture was cooled to ambient temperature, methanol was slowly added under vigorous stirring until the solution became clear. After stirring for another 15 min, removal of the solvents under reduced pressure gave a white residue that was dissolved in 20 mL of aq. KOH solution (20% w/v) and stirred for 15 h at ambient temperature. Adjustment to pH 11 by addition of hydrochloric acid (2 M) was followed by extraction of the aqueous layer with DCM (3 × 25 mL) and a 1:4 mixture of ethanol/chloroform (5 × 25 mL). The combined organic layers were washed with water (3 × 25 mL) and brine (25 mL) and dried over $MgSO_4$. The solvent was removed under reduced pressure to give **8f** (1.22 g, 84%) as a crude yellow oil that was used for the next step without further purification. ^{1}H NMR (DMSO-d_6, 500 MHz): δ = 10.83 (s, 1H), 7.54 (d, J = 7.9 Hz, 1H), 7.34 (d, J = 8.0 Hz, 1H), 7.15 (d, J = 1.8 Hz, 1H), 7.06 (ddt, J = 8.2, 5.0, 1.4 Hz, 1H), 6.99−6.94 (m, 1H), 3.41−3.35 (m, 1H), 3.24 (m, 1H), 3.01 (q, J = 6.1 Hz, 1H), 2.81 (dd, J = 14.2, 6.1 Hz, 1H), 2.60 (dd, J = 14.2, 7.1 Hz, 1H). ^{13}C NMR (DMSO-d_6, 126 MHz): δ = 136.3, 127.58, 123.3, 120.8, 118.4, 118.1, 111.6, 111.3, 65.7, 53.6, 29.4. m/z (ESI): 191.12 ([M + H]$^+$).

(*S*)-4-Bromo-*N*-(1-hydroxy-3-phenylpropan-2-yl)benzenesulfonamide (9a). Synthesis of **9a** was performed by following general procedure A using L-phenylalaninol (**8a**). Yield 98%, colorless solid. ^{1}H NMR (DMSO-d_6, 500 MHz) δ = 7.60−7.56 (m, 2H), 7.50−7.46 (m, 2H), 7.12 (dd, J = 5.2, 1.9 Hz, 3H), 7.06−7.00 (m, 2H), 4.80 (s, 1H), 3.33 (dd, J = 10.1, 4.2 Hz, 1H), 3.30−3.24 (m, 1H), 3.21 (dd, J = 9.9, 6.6 Hz, 1H), 2.83 (dd, J = 13.7, 5.3 Hz, 1H), 2.46 (dd, J = 13.7, 8.0 Hz, 1H). ^{13}C NMR (DMSO-d_6, 126 MHz) δ = 140.9, 138.3, 131.8, 129.1, 128.0, 128.0, 125.7, 125.5, 63.2, 57.3, 37.0. m/z (APCI): 370.01 ([M + H]$^+$).

(*R*)-4-Bromo-*N*-(1-hydroxy-3-phenylpropan-2-yl)benzenesulfonamide (9b). Synthesis of **9b** was performed by following general procedure A using D-phenylalaninol (**8b**). Yield 99%, colorless solid. ^{1}H NMR ($CDCl_3$, 300 MHz): δ = 7.48 (s, 4H), 7.21−7.13 (m, 3H), 7.00−6.93 (m, 2H), 3.69 (dd, J = 11.1, 4.1 Hz, 1H), 3.59 (dd, J = 11.1, 4.6 Hz, 1H), 3.53−3.39 (m, 1H), 2.83 (dd, J = 13.9, 6.3 Hz, 1H), 2.68 (dd, J = 14.0, 8.2 Hz, 1H). m/z (ESI): 370.01 ([M + H]$^+$).

(*S*)-4-Bromo-*N*-(1-hydroxy-3-(4-hydroxyphenyl)propan-2-yl)benzenesulfonamide (9c). To a solution of L-tyrosinol (469 mg, 2.15 mmol) in 10 mL of a 1:1 mixture of water/acetone was added sodium bicarbonate (658 mg, 7.83 mmol), and the mixture was stirred at ambient temperature for 15 min. 4-Bromobenzene-sulfonyl chloride (**1**, 500 mg, 1.96 mmol) was added, and stirring was continued for 17 h. After evaporation of the volatile solvent under reduced pressure, 10 mL of ethyl acetate was added, and the layers were separated. The aqueous layer was extracted with ethyl acetate (3 × 5 mL), and the combined organic layers were washed with saturated $NaHCO_3$ (aq, 3 × 5 mL) and dried over $MgSO_4$. The solvent was removed under reduced pressure to give crude crystals that were recrystallized from methanol to give **9c** (455 mg, 60%) as colorless crystals. ^{1}H NMR (DMSO-d_6, 500 MHz): δ = 9.09 (s, 1H), 7.67 (d, J = 7.3 Hz, 2H), 7.67−7.60 (m, 3H), 7.55−7.49 (m, 2H), 6.87−6.80 (m, 2H), 6.59−6.52 (m, 2H), 4.69 (t, J = 5.1 Hz, 1H), 3.30−3.25 (m, 2H), 3.22−3.14 (m, 2H), 2.69 (dd, J = 13.8, 5.4 Hz, 1H), 2.35 (dd, J = 13.8, 6.9 Hz, 1H). m/z (ESI): 386.01 ([M + H]$^+$).

(*R*)-4-Bromo-*N*-(1-hydroxy-3-(4-hydroxyphenyl)propan-2-yl)benzenesulfonamide (9d). To a solution of D-tyrosinol (**8d**, 229 mg, 1.37 mmol) in 7 mL of a 1:1 mixture of water/acetone was added sodium bicarbonate (460 mg, 5.48 mmol), and the mixture was stirred at ambient temperature for 15 min. 4-Bromobenzenesulfonyl chloride (**1**, 350 mg, 1.37 mmol) was added, and the solution was heated to 40 °C for 4 h. After evaporation of the volatile solvent under reduced pressure, 7 mL of ethyl acetate was added, and the layers were separated. The aqueous layer was extracted with ethyl acetate (3 × 5 mL), and the combined organic layers were washed with saturated $NaHCO_3$ (aq, 3 × 5 mL) and dried over $MgSO_4$. The solvent was removed under reduced pressure to give **9d** (371 mg, 70%) as a crude yellow solid that was used in the next step without further purification. ^{1}H NMR (DMSO-d_6, 300 MHz): δ = 7.68−7.58 (m, 2H), 7.52 (d, J = 8.5 Hz, 2H), 6.88−6.78 (m, 2H), 6.60−6.51 (m, 2H), 4.71 (s, 1H), 3.25−3.12 (m, 4H), 2.69 (dd, J = 13.7, 5.5 Hz, 1H), 2.35 (dd, J = 13.9, 6.9 Hz, 1H). ^{13}C NMR (DMSO-d_6, 75 MHz) δ = 155.6, 141.0, 132.9, 131.8, 130.1, 130.0, 128.2, 114.8, 62.8, 57.4, 36.2. m/z (ESI): 386.01 ([M + H]$^+$).

(*S*)-4-Bromo-*N*-(1-hydroxy-3-(1*H*-indol-3-yl)propan-2-yl)-benzenesulfonamide (9e). To a stirred solution of L-tryptophanol (**8e**, 400 mg, 2.10 mmol) in 40 mL of a 1:2 mixture of DCM/acetonitrile was added *N*,*N*′-diisopropylethylamine (326 mg, 2.52 mmol). The mixture was stirred at ambient temperature for 1 h, and 4-bromobenzene-sulfonyl chloride (**1**, 537 mg, 2.10 mmol) was added in small portions over 30 min at 0 °C under cooling in an ice bath. The cooling bath was removed, and the solution was stirred at ambient temperature for 24 h. Removal of the solvent under reduced pressure gave a brown residue that was taken up in 30 mL of DCM, washed with hydrochloric acid (1 N, 3 × 5 mL), water (3 × 5 mL), and brine (5 mL) and dried over $MgSO_4$. The solvent was removed under reduced pressure to give a crude brown oil that was purified by column chromatography using a 1:1 mixture of ethyl acetate/cyclohexane yielding **9e** (257 mg, 30%) as a yellow oil. ^{1}H NMR (DMSO-d_6, 500 MHz): δ = 10.70 (s, 1H), 7.73 (d, J = 6.9 Hz, 1H), 7.50−7.43 (m, 4H), 7.28 (dt, J = 7.8, 1.0 Hz, 2H), 7.07−7.01 (m, 2H), 6.91 (tt, J = 6.9, 0.9 Hz, 1H), 4.79 (t, J = 5.3 Hz, 1H), 3.42−3.39 (m, 1H), 3.33−3.25 (m, 2H), 2.95 (dd, J = 14.3, 6.0 Hz, 1H), 2.61 (dd, J = 14.3, 7.0 Hz, 1H). ^{13}C NMR (DMSO-d_6, 126 MHz): δ = 140.6, 136.1, 131.4, 127.9, 127.0, 125.4, 123.7, 120.6, 118.1, 117.9, 111.4, 110.3, 63.2, 56.1, 27.0. m/z (ESI): 409.02 ([M + H]$^+$).

(*R*)-4-Bromo-*N*-(1-hydroxy-3-(1*H*-indol-3-yl)propan-2-yl)-benzenesulfonamide (9f). To a stirred solution of D-tryptophanol (**8f**, 625 mg, 3.29 mmol) in 60 mL of a 1:2 mixture of DCM/acetonitrile was added *N*,*N*′-diisopropylethylamine (510 mg, 3.94 mmol). The mixture was stirred at ambient temperature for 1 h, and 4-bromobenzene-sulfonyl chloride (**1**, 839 mg, 3.29 mmol) was added in small portions over 30 min at 0 °C under cooling in an ice bath.

https://dx.doi.org/10.1021/acs.jmedchem.0c02118
J. Med. Chem. XXXX, XXX, XXX−XXX

The cooling bath was removed, and the solution was stirred at ambient temperature for 24 h. Removal of the solvent under reduced pressure gave a brown residue that was taken up in 40 mL of DCM, washed with hydrochloric acid (1 N, 3 × 7 mL), water (3 × 7 mL), and brine (7 mL) and dried over $MgSO_4$. The solvent was removed under reduced pressure to give a crude brown oil that was purified by column chromatography using a 1:1 mixture of ethyl acetate/cyclohexane yielding **9f** (579 mg, 43%) as a yellow oil. ^{1}H NMR (DMSO-d_6, 500 MHz): δ = 10.66 (s, 1H), 7.69 (d, J = 7.0 Hz, 1H), 7.50−7.41 (m, 4H), 7.30−7.23 (m, 2H), 7.05−6.98 (m, 2H), 6.93−6.85 (m, 1H), 4.75 (t, J = 5.4 Hz, 1H), 3.40−3.36 (m, 1H), 3.33−3.24 (m, 2H), 2.94 (dd, J = 14.4, 6.0 Hz, 1H), 2.60 (dd, J = 14.3, 7.0 Hz, 1H). ^{13}C NMR (DMSO-d_6, 126 MHz): δ = 140.6, 136.1, 131.4, 127.9, 127.0, 125.4, 123.7, 120.6, 118.1, 117.9, 111.4, 110.3, 63.2, 56.1, 27.0. m/z (ESI): 409.02 ([M + H]$^+$).

(*S*)-*N*-(1-Hydroxy-3-phenylpropan-2-yl)-4-(1*H*-pyrrolo[2,3-*b*]pyridin-4-yl)benzenesulfonamide (10a). Starting from **9a**, the synthesis of **10a** was performed by following general procedure B. Purification was performed by column chromatography using a 20:1:0.1 mixture of DCM/MeOH/10% aq. NH_4OH (25%) in MeOH. Yield 42%, beige solid. ^{1}H NMR (DMSO-d_6, 500 MHz): δ = 11.90 (s, 1H), 8.35 (d, J = 14.7, 5.0 Hz, 1H), 7.86−7.67 (m, 4H), 7.59 (t, J = 22.3, 3.1 Hz, 1H), 7.28 (d, J = 50.0, 4.9 Hz, 1H), 7.16−6.99 (m, 4H), 6.58 (t, 1H), 4.87 (t, J = 5.5 Hz, 1H), 3.46−3.40 (m, 1H), 3.35−3.31 (m, 1H), 3.31−3.20 (m, 1H), 2.87 (dd, J = 13.6, 5.5 Hz, 1H), 2.47 (d, J = 8.4 Hz, 1H). ^{13}C NMR (DMSO-d_6, 126 MHz): δ = 149.2, 142.9, 141.6, 141.2, 138.6, 138.4, 129.1, 128.6, 128.0, 127.2, 126.8, 125.9, 117.1, 114.31, 98.9, 63.3, 57.3, 37.0. ^{13}C NMR (DMSO-d_6, 126 MHz, DEPT): δ = 142.9, 129.1, 128.6, 128.0, 127.1, 126.8, 125.8, 114.3, 98.8, 63.3, 57.3, 37.1. m/z (ESI): 408.14 ([M + H]$^+$). m/z (ESI-HRMS): 408.1378 ([M + H]$^+$).

(*R*)-*N*-(1-Hydroxy-3-phenylpropan-2-yl)-4-(1*H*-pyrrolo[2,3-*b*]pyridin-4-yl)benzenesulfonamide (10b). Starting from **9b**, the synthesis of **10b** was performed by following general procedure B. Purification was performed by column chromatography using a 20:1:0.1 mixture of DCM/MeOH/10% aq. NH_4OH (25%) in MeOH. Yield 56%, beige solid. ^{1}H NMR (DMSO-d_6, 500 MHz): δ = 11.88 (s, 1H), 8.34 (d, J = 4.9 Hz, 1H), 7.80−7.72 (m, 4H), 7.60 (t, J = 2.9 Hz, 1H), 7.22 (dd, J = 4.9, 1.1 Hz, 1H), 7.15−6.98 (m, 5H), 6.72−6.54 (m, 1H), 4.86 (t, J = 5.4 Hz, 1H), 3.44−3.40 (m, 1H), 3.37−3.32 (m, 1H), 3.28 (dt, J = 11.1, 6.1 Hz, 1H), 2.88 (dd, J = 13.7, 5.4 Hz, 1H), 2.50 (dd, 1H). ^{13}C NMR (DMSO-d_6, 126 MHz): δ = 149.15, 142.95, 141.64, 141.22, 138.63, 138.37, 129.14, 128.59, 127.97, 127.14, 126.76, 125.85, 117.13, 114.32, 98.80, 63.27, 57.28, 37.07. ^{13}C NMR (DMSO-d_6, 126 MHz, DEPT): δ = 143.0, 129.2, 128.6, 128.0, 127.2, 126.8, 125.9, 114.4, 98.8, 63.3, 57.3, 37.1. m/z (ESI): 815.09 ([2M + H]$^+$), 408.14 ([M + H]$^+$). m/z (ESI-HRMS): 408.1374 ([M + H]$^+$).

(*S*)-*N*-(1-Hydroxy-3-(4-hydroxyphenyl)propan-2-yl)-4-(1*H*-pyrrolo[2,3-*b*]pyridin-4-yl)benzenesulfonamide (10c). Starting from **9c**, the synthesis of **10c** was performed by following general procedure B. Purification was performed by column chromatography using a 10:1:0.1 mixture of DCM/MeOH/10% aq. NH_4OH (25%) in MeOH. Yield 51%, colorless solid. ^{1}H NMR (DMSO-d_6, 500 MHz): δ = 11.88 (s, 1H), 9.14 (s, 1H), 8.33 (d, J = 4.9 Hz, 1H), 7.86−7.74 (m, 4H), 7.71 (d, J = 7.3 Hz, 1H), 7.59 (t, J = 3.0 Hz, 1H), 7.26 (d, J = 4.9 Hz, 1H), 6.88 (d, J = 8.5 Hz, 2H), 6.63 (dd, J = 3.6, 1.8 Hz, 1H), 6.58 (d, J = 8.4 Hz, 2H), 4.79 (t, J = 5.3 Hz, 1H), 3.38−3.33 (m, 1H), 3.25 (p, J = 6.1 Hz, 2H), 2.75 (dd, J = 13.7, 5.5 Hz, 1H), 2.40 (dd, J = 13.7, 6.9 Hz, 1H). ^{13}C NMR (DMSO-d_6, 126 MHz): δ = 155.7, 149.2, 143.0, 141.8, 141.4, 138.7, 130.1, 128.6, 128.4, 127.2, 126.9, 117.2, 114.9, 114.48, 98.9, 62.9, 57.5, 36.3. m/z (ESI): 424.13 ([M + H]$^+$). m/z (ESI-HRMS): 424.1326 ([M + H]$^+$).

(*R*)-*N*-(1-Hydroxy-3-(4-hydroxyphenyl)propan-2-yl)-4-(1*H*-pyrrolo[2,3-*b*]pyridin-4-yl)benzenesulfonamide (10d). Starting from **9d**, the synthesis of **10d** was performed by following general procedure B. Purification was performed by column chromatography using a 10:1:0.1 mixture of DCM/MeOH/10% aq. NH_4OH (25%) in MeOH. Yield 26%, colorless solid. ^{1}H NMR (DMSO-d_6, 500 MHz): δ = 11.87 (s, 1H), 9.10 (d, J = 1.3 Hz, 1H), 8.33 (d, J = 4.9 Hz, 1H), 7.86−7.80 (m, 2H), 7.79−7.73 (m, 2H), 7.67 (d, J = 7.0 Hz, 1H), 7.59 (t, J = 2.9 Hz, 1H), 7.26 (dd, J = 5.0, 1.4 Hz, 1H), 6.87 (d, J = 7.1 Hz, 2H), 6.63 (q, J = 3.5, 1.6 Hz, 1H), 6.57 (d, J = 8.4 Hz, 2H), 4.75 (t, J = 5.2 Hz, 1H), 3.31−3.15 (m, 3H), 2.74 (dd, J = 13.7, 5.4 Hz, 1H), 2.40 (dd, J = 13.8, 6.8 Hz, 1H). ^{13}C NMR (DMSO-d_6, 126 MHz): δ = 155.6, 149.1, 142.9, 141.7, 141.3, 138.6, 130.1, 128.6, 128.4, 127.1, 126.9, 117.2, 114.9, 114.4, 98.8, 62.8, 57.4, 36.3. ^{13}C NMR (DMSO-d_6, 126 MHz, DEPT): δ = 142.9, 130.1, 128.6, 127.1, 126.9, 114.9, 114.4, 98.8, 62.8, 36.3. m/z (ESI): 424.13 ([M + H]$^+$). m/z (ESI-HRMS): 424.1328 ([M + H]$^+$).

(*S*)-*N*-(1-Hydroxy-3-(1*H*-indol-3-yl)propan-2-yl)-4-(1*H*-pyrrolo[2,3-*b*]pyridin-4-yl)benzenesulfonamide (10e). Starting from **9e**, the synthesis of **10e** was performed by following general procedure B. Purification was performed by column chromatography using a 20:1:0.1 mixture of DCM/MeOH/10% aq. NH_4OH (25%) in MeOH. Yield 60%, beige solid. ^{1}H NMR (DMSO-d_6, 500 MHz,): δ = 11.85 (s, 1H), 10.69 (s, 1H), 8.32 (d, J = 4.9 Hz, 1H), 7.79−7.73 (m, 4H), 7.70 (d, J = 6.5 Hz, 1H), 7.57 (t, J = 2.9 Hz, 1H), 7.31 (d, J = 7.9 Hz, 1H), 7.20 (dd, J = 7.0, 5.3 Hz, 2H), 7.07 (d, J = 1.8 Hz, 1H), 6.93 (td, J = 8.1, 1.3 Hz, 1H), 6.86 (t, J = 7.4 Hz, 1H), 6.59 (dd, J = 3.4, 1.7 Hz, 1H), 4.74 (s, 1H), 3.42−3.38 (m, 2H), 3.37−3.26 (m, 2H), 2.97 (dd, J = 14.3, 6.4 Hz, 1H), 2.67 (dd, J = 14.3, 6.0 Hz, 1H). ^{13}C NMR (DMSO-d_6, 126 MHz): δ = 149.1, 142.8, 141.6, 141.2, 138.6, 136.1, 128.4, 127.2, 127.1, 126.8, 123.8, 120.7, 118.1, 118.0, 117.1, 114.40, 111.3, 110.4, 98.9, 62.9, 56.2, 27.1. ^{13}C NMR (DMSO-d_6, 126 MHz, DEPT): δ = 142.9, 128.4, 127.1, 126.8, 123.8, 120.7, 118.1, 118.0, 114.4, 111.3, 98.9, 62.9, 56.2, 27.1. m/z (ESI): 447.15 ([M + H]$^+$). m/z (ESI-HRMS): 447.1484 ([M + H]$^+$).

(*R*)-*N*-(1-Hydroxy-3-(1*H*-indol-3-yl)propan-2-yl)-4-(1*H*-pyrrolo[2,3-*b*]pyridin-4-yl)benzenesulfonamide (10f). Starting from **9f**, the synthesis of **10f** was performed by following general procedure B. Purification was performed by column chromatography using a 20:1:0.1 mixture of DCM/MeOH/10% aq. NH_4OH (25%) in MeOH. Yield 62%, beige solid. ^{1}H NMR (DMSO-d_6, 500 MHz): δ = 11.86 (s, 1H), 10.71 (s, 1H), 8.33 (d, J = 4.9 Hz, 1H), 7.79−7.74 (m, 4H), 7.71 (d, J = 7.0 Hz, 1H), 7.58 (dd, J = 3.5, 2.6 Hz, 1H), 7.32 (d, J = 7.0 Hz, 1H), 7.22 (d, J = 4.9 Hz, 1H), 7.20 (d, J = 8.2 Hz, 1H), 7.08 (d, J = 2.3 Hz, 1H), 6.94 (ddd, J = 8.1, 7.0, 1.1 Hz, 1H), 6.87 (ddd, J = 7.9, 7.0, 1.0 Hz, 1H), 6.60 (dd, J = 3.5, 1.9 Hz, 1H), 4.76 (t, J = 5.4 Hz, 1H), 3.41−3.37 (m, 2H), 3.32−3.29 (m, 1H), 2.98 (dd, J = 14.3, 6.5 Hz, 1H), 2.67 (dd, J = 14.3, 6.2 Hz, 1H). ^{13}C NMR (DMSO-d_6, 126 MHz): δ = 149.2, 142.9, 141.6, 141.2, 138.6, 136.1, 128.4, 127.2, 127.1, 126.8, 123.8, 120.7, 118.1, 118.0, 117.1, 114.4, 111.3, 110.4, 98.9, 62.9, 56.2, 27.0. m/z (ESI): 893.29 ([2M + H]$^+$), 447.15 ([M + H]$^+$). m/z (ESI-HRMS): 447.1485 ([M + H]$^+$).

Molecular Modeling. Molecular modeling was performed using the Molecular Operating Environment (Molecular Operating Environment MOE, 2016.0802; Chemical Computing Group ULC, 1010 Sherbooke St. West, Suite #910, Montreal, QC, Canada, H3A 2R7, 2021) software package, employing an "Amber10" force field.

Isolation of the monomeric kinase domains was achieved by manual deletion of the bridged chain using the "sequence editor". Superposition of the isolated chains was performed with the "align/superpose" tool of the "sequence editor".

Reconstruction of the glycine-rich loop (P-Loop) was performed using the "SuperLooper2" web server.[47] Starting from the crystal structure of Nek1 (PDB code 4B9D.B), the missing loop sequence EGSFG (between G11 and K17) was reconstructed by using the AGPAG loop (between P311 and R317) of the *Mycobacterium tuberculosis* probable periplasmic sugar-binding lipoprotein UspC (PDB code 5K2Y) crystal structure as a template.

The Nek1 kinase domain homology model was created using the "homology model" function and the crystal structure of Nek2 bound to an aminopurine inhibitor (PDB code 5M53) as the template.[48]

For all docking experiments, residual water molecules were deleted, and the receptors were prepared using the "QuickPrep" function without "automated structure preparation". Using the respective functions of the "MOE Database Viewer", all ligands were "washed" before partial charges were determined and the structures underwent energy minimization. The binding sites were designated from the

https://dx.doi.org/10.1021/acs.jmedchem.0c02118
J. Med. Chem. XXXX, XXX, XXX−XXX

cocrystallized ligand (PDB code 4B9D), which was placed in the binding site by superposition in the case of the apo structure (PDB code 4APC) and the homology model. Docking poses were placed using the "Triangle Matcher" method and scored by a "London dG" function. Refinements of the poses were performed by using the "Rigid Receptor" method and were finally scored using a "GBVI/WSA dG" function. For the docking of **3a** into the apo structure, a hinge binding pharmacophore was defined, based on the cocrystallized ligand.

The sequence homology analysis between the human and zebrafish Nek1 kinase domains was performed using the "MOE protein similarity monitor". Identity and similarity values are equal to the number of matches divided by the number of amino acids in the chain corresponding to the cell column. Residues are considered similar if their BLOSUM62 scores are greater than zero.

In accordance with the author guidelines, all virtual screening hits were filtered for PAINS using the PAINS-remover online application.[64] All compounds passed the filter.

***In Vitro* Kinase Activity Assays.** Residual kinase inhibition was determined with the commercial Eurofins Discovery KinaseProfiler service at 1 μM compound concentration and either 10 μM ATP or an ATP concentration within 15 μM of the apparent K_m for ATP (see Supporting Information for K_m values). In the case of Nek1 (KinaseProfiler ITEM 15-020KP10 and ITEM 15-020KP), recombinant human Nek1 (1−505) was incubated with 8 mM MOPS (pH 7.0), 0.2 mM EDTA, 250 μM RLGRDKYKTLRQIRQ, 10 mM magnesium acetate, and [γ-^{33}P-ATP]. The reaction was initiated by the addition of the Mg/ATP mix. After incubation for 40 min at room temperature, the reaction was stopped by the addition of phosphoric acid to a concentration of 0.5%. Ten microliters of the reaction was then spotted onto a P30 filtermat and washed four times for 4 min in 0.425% phosphoric acid and once in methanol prior to drying and scintillation counting. Values are the mean from two independent experiments.

IC_{50} values for Nek1 and Nek2 were determined in a TR-FRET based activity assays (LANCE Ultra TR-FRET, PerkinElmer) at an ATP concentration within 15 μM of the apparent K_m for ATP in the respective assay format (60 μM for both Nek1 and Nek2). The IC_{50} curves consist of 10 test compound concentrations tested at half-log dilutions from 30 μM to 1 nM with vehicle and inhibitory control wells. For compounds **3j** and **3k**, the maximum concentration was set to 10 μM as a consequence of solubility issues at 30 μM, and the respective IC_{50} curves consist of 9 test compound concentrations tested at half-log dilutions from 10 μM to 1 nM. Values are the mean from two independent experiments. Recombinant human Nek1 (1−505; 0.02 nM) or Nek2 (full length; 0.2 nM) (both from Thermo Fisher Scientific) was incubated with 50 mM HEPES (pH 7.5), 1 mM EGTA, 10 mM $MgCl_2$, 0.2 mM DTT, 0.01% Tween20, and 50 nM ULight-p70 S6K (Thr389) peptide (sequence LGFTYVAP; PerkinElmer). The reaction was initiated by the addition of the p70 S6K peptide/ATP mix. After incubation for 30 min at 22 °C, the reaction was stopped by the addition of 10 mM EDTA and 0.3 nM europium-antiphospho-p70 S6K (Thr389) antibody in CR97 detection buffer (both PerkinElmer). After incubation for 1 h at 22 °C for signal development, the plates were analyzed in a plate reader (PHERAstar FSX, BMG LABTECH). For compounds **3g** and **3k**, relative IC_{50} values were provided instead of absolute IC_{50}, as the determined IC_{50} values exceeded the employed maximum test concentrations (30 μM for **3g**, 10 μM for **3k**).

For compounds **3a**, **3f**, **10a−f**, IC_{50} values were also determined with the Eurofins Discovery IC50Profiler service at either 10 μM (ITEM 15-020KP10) or an ATP concentration within 15 μM of the apparent K_m for ATP (90 μM, ITEM 15-020KP). The IC_{50} curves consist of 9 test compound concentrations tested at half-log dilutions from 10 μM to 1 nM with vehicle control wells. Values are the mean from two independent experiments.

IC_{50} values and 95% confidence intervals were determined from the raw data provided in the Supporting Information by nonlinear regression (log_inhibitor vs response_variable slope_four parameters) using GraphPad Prism, version 8.4.3 (471) for OS X, (GraphPad Software, San Diego, California USA, www.graphpad.com). For compounds **3j** and **3k**, the maximum concentration data points were dropped, as a consequence of solubility issues at 30 μM.

Caco-2 Cell Permeability Assay. A−B permeability (Caco-2, pH 6.5/7.4) and percent recovery were determined by HPLC-MS/MS detection of the peak area response in a commercial assay by Eurofins Discovery Services (Item 3318). Propranolol, labetalol, colchicine, and ranitidine were tested concurrently as reference compounds.

Fish Maintenance and Husbandry Protocols. Fish maintenance and husbandry protocols were documented and approved by the Darmstadt administrative authority. All animals were treated humanely in accordance with the German animal protection standards and the EU Directive 2010/63/EU of the European parliament and of the council. Adult wild-type zebrafish (*Danio rerio*) were maintained in 60 L fish tanks in a laboratory with no daylight and a constant temperature of 28 °C. Room light was programmed to a 12 h dark/12 h light cycle. Adult zebrafish were bred in mating containers (2 animals/1 L) or mating tanks (6−8 animals/20 L) that were equipped with plastic grass and a removable sieve at the bottom of the tank. Embryos were collected 2−3 h after a light cycle started, rinsed with E3-medium, and isolated in Petri dishes containing E3-medium. E3-medium was prepared according to the Cold Spring Harbor Protocols recipe for E3 medium for zebrafish embryos (doi: 10.1101/pdb.rec066449).

Zebrafish Developmental Toxicity Assay. The aqueous solubility of **10f** was determined in a shake-flask HPLC solubility assay using the previously described HPLC system connected to a diode array detector (DAD, see General Information). Absorption was measured at 280 nm, and all measurements were performed in triplicate. A saturated solution of **10f** in E3-medium was prepared by shaking for 24 h at 25 °C. A 10 mM stock solution of **10f** in DMSO was diluted to 1, 5, 10, 50, and 100 μM solutions in acetonitrile, and the aqueous solubility of **10f** was determined by interpolation using Prism 8 by GraphPad Software, LLC.

The zebrafish developmental toxicity screen was performed in accordance to guidelines published by M. Haldi et al. in *Zebrafish: Methods for Assessing Drug Saftey and Toxicity*.[65]

At 4 hpf (hours postfertilization), 15 embryos per group (0.05, 0.1, 0.5, 1.5, 2.5, 5, 10, 15, 20, 30 μM) that exhibited intact chorion membranes were selected and reexamined after 2 h. A stock solution (10 mM in DMSO) of the test compound was diluted to 10× final concentrations, and the embryos were sorted in 180 μL of E3 medium. At 6 hpf, 20 μL of the 10× solution was added to give the final concentrations. Survival was monitored every 24 h by observation of the heartbeat. All survival rates were determined at least in triplicate with the controls and the survival rate at 30 μM being determined in 5 replicates.

Stability-Indicating HPLC Assay. The stability-indicating HPLC assay was performed using the previously described HPLC system connected to a diode array detector (DAD, see General Information). A 15 μM solution of **10f** in E3-medium containing 75 μM 2-phenylthiourea (PTU) and a 15 μM solution of **10f** containing 75 μM PTU and 2.5 μM PT-Yellow (BDNCA3-D2) were prepared for HPLC injection. Absorptions were measured every 24 h at 280 nm for compound **10f** and PTU and 548 nm for PT-Yellow over 48 or 120 h, respectively. All measurements were performed in triplicate.

Fluorescence Microscopy Imaging of Zebrafish Pronephroi. The 96-well plate molding tool was manufactured by selective laser melting on an EOS M290 (EOS GmbH Electro Optical Systems, Krailing, Germany) metal 3D-printing system using EOS Stainless-Steel 316L as the material with a layer height of 20 μM. The tool consists of a base plate with 96 perpendicular pins that match the positions of the wells of a microtiter plate. The agarose molds were prepared using 1% NEEO ultraquality agarose (Carl Roth, Karlsruhe, Germany, Art. No. 2267.1) in black-walled 96-well Nunc polymer optical bottom plates (Thermo Fisher Scientific, Waltham, Massachusetts, USA). The specifications of the molding tool and the preparation of the agarose molds in 96-well microtiter plates followed the procedure published by Westhoff et al.[55]

https://dx.doi.org/10.1021/acs.jmedchem.0c02118
J. Med. Chem. XXXX, XXX, XXX−XXX

Image Acquisition. Imaging of fluorescently labeled (PT-Yellow) zebrafish embryos was performed on an Olympus IX-81 widefield microscope (Olympus, Shinjuku, Tokyo, Japan), using an Olympus CPlanFL N, 10×, NA 0.3 objective in combination with a 1.5× tube lens magnification, resulting in a total magnification of 15×. Fluorescence was excited using a CoolLED pE300 Ultra (CoolLED Ltd., Andover, NY, USA) and detected on a pco.edge 5.5 (PCO AG, Kelheim, Germany) using appropriate filter sets. The whole setup was controlled using Micromanager 1.4.22.[66] to record 33 *Z*-slices with a *Z*-distance of 15 μm per embryo after manual orientation in the previously described agarose molds.

Image Processing and Deconvolution. Image processing was performed using ImageJ, version 2.0.0.-rc-69/1.52p. Deconvolution was performed using the DeconvolutionLab2 plugin and a point spread function that was simulated in the PSF Generator plugin. The image stacks are presented as colored maximum *Z*-projections using the lookup table *blue orange icb* (Figure S14). As it was not possible to remove all out of focus blur with the deconvolution procedure, the sharpest 5 consecutive *Z*-slices of labeled pronephrons were manually selected in each stack (Figures S15 and S16). Subsequently, the following image analysis steps were applied using ImageJ: (1) subtract background using a 150 pixel rolling ball, (2) sum all 5 images into one, (3) threshold images above 100, (4) convert background to 8-bit mask for the intensity quantification or convert background to NaN for the quantification of the pronephron areas. The pronephron area in the summed stacks was used as the quantity to estimate the size of the pronephroi.

■ ASSOCIATED CONTENT

Supporting Information

The Supporting Information is available free of charge at https://pubs.acs.org/doi/10.1021/acs.jmedchem.0c02118.

Molecular modeling, homology model coordinates, *in vitro* pharmacology, NMR data, lead compound HPLC traces, bioavailability profile of compound **10f** (PDF)

Molecular formula strings (CSV)

Nek1 homology model (PDB)

Superlooper2 reconstruction model (PDB)

■ AUTHOR INFORMATION

Corresponding Authors

Boris Schmidt − *Clemens Schöpf−Institute of Organic Chemistry and Biochemistry, Technische Universität Darmstadt, 64287 Darmstadt, Germany*; orcid.org/0000-0003-1662-2392; Phone: +496151-1623745; Email: schmidt_boris@t-online.de; Fax: +496151-163278

Georg Baumann − *Clemens Schöpf−Institute of Organic Chemistry and Biochemistry, Technische Universität Darmstadt, 64287 Darmstadt, Germany*; Email: georg.baumann@stud.tu-darmstadt.de

Authors

Tobias Meckel − *Clemens Schöpf−Institute of Organic Chemistry and Biochemistry, Technische Universität Darmstadt, 64287 Darmstadt, Germany*

Kevin Böhm − *Clemens Schöpf−Institute of Organic Chemistry and Biochemistry, Technische Universität Darmstadt, 64287 Darmstadt, Germany*

Yung-Hsin Shih − *Clemens Schöpf−Institute of Organic Chemistry and Biochemistry, Technische Universität Darmstadt, 64287 Darmstadt, Germany*

Mirco Dickhaut − *Clemens Schöpf−Institute of Organic Chemistry and Biochemistry, Technische Universität Darmstadt, 64287 Darmstadt, Germany*

Torben Reichardt − *Clemens Schöpf−Institute of Organic Chemistry and Biochemistry, Technische Universität Darmstadt, 64287 Darmstadt, Germany*

Johannes Pilakowski − *Clemens Schöpf−Institute of Organic Chemistry and Biochemistry, Technische Universität Darmstadt, 64287 Darmstadt, Germany*

Ulrich Pehl − *Merck Healthcare KGaA, Biopharma R&D, Discovery and Development Technologies, 64293 Darmstadt, Germany*

Complete contact information is available at: https://pubs.acs.org/10.1021/acs.jmedchem.0c02118

Author Contributions

G.B., B.S., and T.M. conceived and designed the experiments. G.B., T.M., and B.S. wrote the manuscript. G.B., K.B., Y.S., M.D., U.D., and T.R. performed the experiments. G.B., B.S., U.P., and T.M. analyzed the data. G.B., B.S., T.M., and J.P. gave scientific advice. All authors contributed to the article and approved the submitted version.

Funding

The authors declare that this study received funding from the German Research Foundation (DFG, GRK1657, Project number: 161030019). The funders had no role in study design, data collection and analysis, decision to publish, or preparation of the manuscript.

Notes

The authors declare no competing financial interest.

■ ACKNOWLEDGMENTS

We thank Holger Hermann Merschroth for the design and production of the 96-well plate molding tool and Nadine Herget and Friedrich Baumgärtner for performing the TR-FRET *in vitro* kinase activity assays. We furthermore thank Prof. Markus Löbrich, Julian Spies, and Michael Ensminger for discussions on the biological role of Nek1.

■ ABBREVIATIONS

ALS, amyotrophic lateral sclerosis; CDK, cyclin-dependent kinase; Chk1, checkpoint kinase 1; Chk2, checkpoint kinase 2; cDNA, complementary DNA; DDR, DNA damage response; HR, homologous recombination; IKK, IκB kinase; JNK, c-Jun N-terminal kinase; DSB, double strand break; HR, homologous recombination; Nek1, NIMA-related kinase 1; NF-κB, nuclear factor kappa-light-chain-enhancer of activated B-cells; MOE, Molecular Operating Environment; NIMA, never-in-mitosis gene A; PKD, polycystic kidney disease; PSF, point square function; RCC, renal cell carcinoma; SAR, structure−activity relationship; TLC, thin layer chromatography; TPSA, topological polar surface area; Tlk1, tousled-like kinase 1

■ REFERENCES

(1) van de Kooij, B.; Creixell, P.; van Vlimmeren, A.; Joughin, B. A.; Miller, C. J.; Haider, N.; Simpson, C. D.; Linding, R.; Stambolic, V.; Turk, B. E.; Yaffe, M. B. Comprehensive substrate specificity profiling of the human Nek kinome reveals unexpected signaling outputs. *eLife* **2019**, *8*, No. e44635.

(2) Letwin, K.; Mizzen, L.; Motro, B.; Ben-David, Y.; Bernstein, A.; Pawson, T. A mammalian dual specificity protein kinase, Nek1, is related to the NIMA cell cycle regulator and highly expressed in meiotic germ cells. *EMBO J.* **1992**, *11*, 3521−3531.

(3) Meirelles, G. V.; Perez, A. M.; Souza, E. E.; Basei, F. L.; Papa, P. F.; Melo Hanchuk, T. D.; Cardoso, V. B.; Kobarg, J. Stop Ne(c)king around": How interactomics contributes to functionally characterize

Nek family kinases. *World journal of biological chemistry* **2014**, *5*, 141−160.
(4) Peres de Oliveira, A.; Kazuo Issayama, L.; Betim Pavan, I. C.; Riback Silva, F.; Diniz Melo-Hanchuk, T.; Moreira Simabuco, F.; Kobarg, J. Checking NEKs: Overcoming a Bottleneck in Human Diseases. *Molecules* **2020**, *25*, 1778.
(5) Janaswami, P. M.; Birkenmeier, E. H.; Cook, S. A.; Rowe, L. B.; Bronson, R. T.; Davisson, M. T. Identification and genetic mapping of a new polycystic kidney disease on mouse chromosome 8. *Genomics* **1997**, *40*, 101−107.
(6) Upadhya, P.; Birkenmeier, E. H.; Birkenmeier, C. S.; Barker, J. E. Mutations in a NIMA-related kinase gene cause pleiotropic effects including a progressive polycystic kidney disease in mice. *Proc. Natl. Acad. Sci. U. S. A.* **2000**, *97*, 217−221.
(7) Chebib, F. T.; Torres, V. E. Recent advances in the management of autosomal dominant polycystic kidney disease. *Clin. J. Am. Soc. Nephrol.* **2018**, *13*, 1765−1776.
(8) Surpili, M. J.; Delben, T. M.; Kobarg, J. Identification of proteins that interact with the central coiled-coil region of the human protein kinase NEK1. *Biochemistry* **2003**, *42*, 15369−15376.
(9) Chen, Y.; Chiang, H.-C.; Litchfield, P.; Pena, M.; Juang, C.; Riley, D. J. Expression of Nek1 during kidney development and cyst formation in multiple nephron segments in the Nek1-deficient kat2J mouse model of polycystic kidney disease. *J. Biomed. Sci.* **2014**, *21*, 63−65.
(10) Thiel, C.; Kessler, K.; Giessl, A.; Dimmler, A.; Shalev, S. A.; von der Haar, S.; Zenker, M.; Zahnleiter, D.; Stöss, H.; Beinder, E.; Abou Jamra, R.; Ekici, A. B.; Schröder-Kreß, N.; Aigner, T.; Kirchner, T.; Reis, A.; Brandstätter, J. H.; Rauch, A. NEK1 mutations cause short-rib polydactyly syndrome type Majewski. *Am. J. Hum. Genet.* **2011**, *88*, 106−114.
(11) Monroe, G. R.; Kappen, I. F. P. M.; Stokman, M. F.; Terhal, P. A.; van den Boogaard, M.-J. H.; Savelberg, S. M. C.; van der Veken, L. T.; van Es, R. J. J.; Lens, S. M.; Hengeveld, R. C.; Creton, M. A.; Janssen, N. G.; Mink van der Molen, A. B.; Ebbeling, M. B.; Giles, R. H.; Knoers, N. V.; van Haaften, G. Compound heterozygous NEK1 variants in two siblings with oral-facial-digital syndrome type II (Mohr syndrome). *Eur. J. Hum. Genet.* **2016**, *24*, 1752−1760.
(12) Brenner, D.; Müller, K.; Wieland, T.; Weydt, P.; Böhm, S.; Lulé, D.; Hübers, A.; Neuwirth, C.; Weber, M.; Borck, G.; Wahlqvist, M.; Danzer, K. M.; Volk, A. E.; Meitinger, T.; Strom, T. M.; Otto, M.; Kassubek, J.; Ludolph, A. C.; Andersen, P. M.; Weishaupt, J. H. NEK1 mutations in familial amyotrophic lateral sclerosis. *Brain* **2016**, *139*, No. e28.
(13) Higelin, J.; Catanese, A.; Semelink-Sedlacek, L. L.; Oeztuerk, S.; Lutz, A.-K.; Bausinger, J.; Barbi, G.; Speit, G.; Andersen, P. M.; Ludolph, A. C.; Demestre, M.; Boeckers, T. M. NEK1 loss-of-function mutation induces DNA damage accumulation in ALS patient-derived motoneurons. *Stem Cell Res.* **2018**, *30*, 150−162.
(14) Fry, A. M.; O'Regan, L.; Sabir, S. R.; Bayliss, R. Cell cycle regulation by the NEK family of protein kinases. *J. Cell Sci.* **2012**, *125*, 4423−4433.
(15) Polci, R.; Peng, A.; Chen, P.-L.; Riley, D. J.; Chen, Y. NIMA-related protein kinase 1 is involved early in the ionizing radiation-induced DNA damage response. *Cancer Res.* **2004**, *64*, 8800−8803.
(16) Grudzenski, S.; Raths, A.; Conrad, S.; Rübe, C. E.; Löbrich, M. Inducible response required for repair of low-dose radiation damage in human fibroblasts. *Proc. Natl. Acad. Sci. U. S. A.* **2010**, *107*, 14205−14210.
(17) Spies, J.; Waizenegger, A.; Barton, O.; Surder, M.; Wright, W. D.; Heyer, W.-D.; Lobrich, M. Nek1 regulates Rad54 to orchestrate homologous recombination and replication fork stability. *Mol. Cell* **2016**, *62*, 903−917.
(18) Chen, Y.; Chen, P.-L.; Chen, C.-F.; Jiang, X.; Riley, D. J. Never-in-mitosis related kinase 1 functions in DNA damage response and checkpoint control. *Cell Cycle* **2008**, *7*, 3194−3201.
(19) Chen, Y.; Chen, C.-F.; Riley, D. J.; Chen, P.-L. Nek1 kinase functions in DNA damage response and checkpoint control through a pathway independent of ATM and ATR. *Cell Cycle* **2011**, *10*, 655−663.
(20) Chen, Y.; Craigen, W. J.; Riley, D. J. Nek1 regulates cell death and mitochondrial membrane permeability through phosphorylation of VDAC1. *Cell Cycle* **2009**, *8*, 257−267.
(21) Chen, Y.; Gaczynska, M.; Osmulski, P.; Polci, R.; Riley, D. J. Phosphorylation by Nek1 regulates opening and closing of voltage dependent anion channel 1. *Biochem. Biophys. Res. Commun.* **2010**, *394*, 798−803.
(22) Singh, V.; Khalil, M. I.; De Benedetti, A. The TLK1/Nek1 axis contributes to mitochondrial integrity and apoptosis prevention via phosphorylation of VDAC1. *Cell Cycle* **2020**, *19*, 363−375.
(23) Singh, V.; Jaiswal, P. K.; Ghosh, I.; Koul, H. K.; Yu, X.; De Benedetti, A. The TLK1-Nek1 axis promotes prostate cancer progression. *Cancer Lett.* **2019**, *453*, 131−141.
(24) Singh, V.; Jaiswal, P. K.; Ghosh, I.; Koul, H. K.; Yu, X.; De Benedetti, A. Targeting the TLK1/NEK1 DDR axis with Thioridazine suppresses outgrowth of androgen independent prostate tumors. *Int. J. Cancer* **2019**, *145*, 1055−1067.
(25) Singh, V.; Connelly, Z. M.; Shen, X.; De Benedetti, A. Identification of the proteome complement of humanTLK1 reveals it binds and phosphorylates NEK1 regulating its activity. *Cell Cycle* **2017**, *16*, 915−926.
(26) Melo-Hanchuk, T. D.; Martins, M. B.; Cunha, L. L.; Soares, F. A.; Ward, L. S.; Vassallo, J.; Kobarg, J. Expression of the NEK family in normal and cancer tissue: an immunohistochemical study. *BMC Cancer* **2020**, *20*, 23.
(27) Zhu, J.; Cai, Y.; Liu, P.; Zhao, W. Frequent Nek1 overexpression in human gliomas. *Biochem. Biophys. Res. Commun.* **2016**, *476*, 522−527.
(28) Chen, Y.; Chen, C.-F.; Polci, R.; Wei, R.; Riley, D. J.; Chen, P.-L. Increased Nek1 expression in renal cell carcinoma cells is associated with decreased sensitivity to DNA-damaging treatment. *Oncotarget* **2014**, *5*, 4283−4294.
(29) Wei, R. L.; Chen, Y. Overexpression of Nek1 in renal cell carcinoma protects against cell death from ionizing radiation. *Int. J. Radiat. Oncol., Biol., Phys.* **2011**, *81*, S712.
(30) Freund, I.; Hehlgans, S.; Martin, D.; Ensminger, M.; Fokas, E.; Rödel, C.; Löbrich, M.; Rödel, F. Fractionation-dependent radiosensitization by molecular targeting of Nek1. *Cells* **2020**, *9*, 1235.
(31) Chen, Y. NEK1 protein kinase as a target for anticancer therapeutics. *Chemotherapy: Open Access* **2012**, *1*, e118.
(32) Moraes, E.; Meirelles, G.; Honorato, R.; de Souza, T.; de Souza, E.; Murakami, M.; de Oliveira, P.; Kobarg, J. Kinase inhibitor profile for human nek1, nek6, and nek7 and analysis of the structural basis for inhibitor specificity. *Molecules* **2015**, *20*, 1176−1191.
(33) Melo-Hanchuk, T. D.; Slepicka, P. F.; Meirelles, G. V.; Basei, F. L.; Lovato, D. V.; Granato, D. C.; Pauletti, B. A.; Domingues, R. R.; Leme, A. F. P.; Pelegrini, A. L.; Lenz, G.; Knapp, S.; Elkins, J. M.; Kobarg, J. NEK1 kinase domain structure and its dynamic protein interactome after exposure to Cisplatin. *Sci. Rep.* **2017**, *7*, 5445.
(34) Wells, C. I.; Kapadia, N. R.; Counago, R. M.; Drewry, D. H. In depth analysis of kinase cross screening data to identify chemical starting points for inhibition of the Nek family of kinases. *MedChemComm* **2018**, *9*, 44−66.
(35) De Donato, M.; Righino, B.; Filippetti, F.; Battaglia, A.; Petrillo, M.; Pirolli, D.; Scambia, G.; De Rosa, M. C.; Gallo, D. Identification and antitumor activity of a novel inhibitor of the NIMA-related kinase NEK6. *Sci. Rep.* **2018**, *8*, 16047.
(36) Drewry, D. H.; Wells, C. I.; Andrews, D. M.; Angell, R.; Al-Ali, H.; Axtman, A. D.; Capuzzi, S. J.; Elkins, J. M.; Ettmayer, P.; Frederiksen, M.; Gileadi, O.; Gray, N.; Hooper, A.; Knapp, S.; Laufer, S.; Luecking, U.; Michaelides, M.; Müller, S.; Muratov, E.; Denny, R. A.; Saikatendu, K. S.; Treiber, D. K.; Zuercher, W. J.; Willson, T. M. Progress towards a public chemogenomic set for protein kinases and a call for contributions. *PLoS One* **2017**, *12*, No. e0181585.
(37) Seefeld, M. A.; Rouse, M. B.; McNulty, K. C.; Sun, L.; Wang, J.; Yamashita, D. S.; Luengo, J. I.; Zhang, S.; Minthorn, E. A.; Concha, N. O.; Heerding, D. A. Discovery of 5-pyrrolopyridinyl-2-thiophenecar-

https://dx.doi.org/10.1021/acs.jmedchem.0c02118
J. Med. Chem. XXXX, XXX, XXX−XXX

boxamides as potent AKT kinase inhibitors. *Bioorg. Med. Chem. Lett.* **2009**, *19*, 2244−2248.
(38) Liddle, J.; Bamborough, P.; Barker, M. D.; Campos, S.; Cousins, R. P. C.; Cutler, G. J.; Hobbs, H.; Holmes, D. S.; Ioannou, C.; Mellor, G. W.; Morse, M. A.; Payne, J. J.; Pritchard, J. M.; Smith, K. J.; Tape, D. T.; Whitworth, C.; Williamson, R. A. 4-Phenyl-7-azaindoles as potent and selective IKK2 inhibitors. *Bioorg. Med. Chem. Lett.* **2009**, *19*, 2504−2508.
(39) Gehrig, J.; Pandey, G.; Westhoff, J. H. Zebrafish as a model for drug screening in genetic kidney diseases. *Frontiers in Pediatrics* **2018**, *6*, 183.
(40) Bamborough, P.; Barker, M. D.; Campos, S. A.; Cousins, R. P. C.; Faulder, P.; Hobbs, H.; Holmes, D. S.; Johnston, M. J.; Liddle, J.; Payne, J. J.; Pritchard, J. M.; Whitworth, C. Pyrrolo[2,3-b]pyridin-4-yl-benzenesulfonamide compounds as IKK2 inhibitors and their preparation, pharmaceutical compositions and use in the treatment of diseases. WO2008034860A1, 2008.
(41) McKennon, M. J.; Meyers, A. I.; Drauz, K.; Schwarm, M. A convenient reduction of amino acids and their derivatives. *J. Org. Chem.* **1993**, *58*, 3568−3571.
(42) Chong, H.-S.; Song, H. A.; Dadwal, M.; Sun, X.; Sin, I.; Chen, Y. Efficient synthesis of functionalized aziridinium salts. *J. Org. Chem.* **2010**, *75*, 219−221.
(43) Westwood, I.; Cheary, D.-M.; Baxter, J. E.; Richards, M. W.; van Montfort, R. L. M.; Fry, A. M.; Bayliss, R. Insights into the conformational variability and regulation of human Nek2 kinase. *J. Mol. Biol.* **2009**, *386*, 476−485.
(44) Haq, T.; Richards, M. W.; Burgess, S. G.; Gallego, P.; Yeoh, S.; O'Regan, L.; Reverter, D.; Roig, J.; Fry, A. M.; Bayliss, R. Mechanistic basis of Nek7 activation through Nek9 binding and induced dimerization. *Nat. Commun.* **2015**, *6*, 8771.
(45) Irie, T.; Sawa, M. 7-Azaindole: A versatile scaffold for developing kinase inhibitors. *Chem. Pharm. Bull.* **2018**, *66*, 29−36.
(46) Juchum, M.; Günther, M.; Döring, E.; Sievers-Engler, A.; Lämmerhofer, M.; Laufer, S. Trisubstituted imidazoles with a rigidized hinge binding motif act as single digit nM inhibitors of clinically relevant EGFR L858R/T790M and L858R/T790M/C797S mutants: An example of target hopping. *J. Med. Chem.* **2017**, *60*, 4636−4656.
(47) Ismer, J.; Rose, A. S.; Tiemann, J. K. S.; Goede, A.; Preissner, R.; Hildebrand, P. W. SL2: an interactive webtool for modeling of missing segments in proteins. *Nucleic Acids Res.* **2016**, *44*, W390−W394.
(48) Coxon, C. R.; Wong, C.; Bayliss, R.; Boxall, K.; Carr, K. H.; Fry, A. M.; Hardcastle, I. R.; Matheson, C. J.; Newell, D. R.; Sivaprakasam, M.; Thomas, H.; Turner, D.; Yeoh, S.; Wang, L. Z.; Griffin, R. J.; Golding, B. T.; Cano, C. Structure-guided design of purine-based probes for selective Nek2 inhibition. *Oncotarget* **2017**, *8*, 19089−19124.
(49) Roskoski, R. Classification of small molecule protein kinase inhibitors based upon the structures of their drug-enzyme complexes. *Pharmacol. Res.* **2016**, *103*, 26−48.
(50) Smyth, L. A.; Collins, I. Measuring and interpreting the selectivity of protein kinase inhibitors. *Journal of Chemical Biology* **2009**, *2*, 131−151.
(51) Outtandy, P.; Russell, C.; Kleta, R.; Bockenhauer, D. Zebrafish as a model for kidney function and disease. *Pediatr. Nephrol.* **2019**, *34*, 751−762.
(52) Wlodarchak, N.; Tariq, R.; Striker, R. Comparative analysis of the human and zebrafish kinomes: focus on the development of kinase inhibitors. *Trends Cell Mol. Biol.* **2015**, *10*, 49−75.
(53) Knight, Z. A.; Shokat, K. M. Chemical Genetics: Where Genetics and Pharmacology Meet. *Cell* **2007**, *128*, 425−430.
(54) Shalom, O.; Shalva, N.; Altschuler, Y.; Motro, B. The mammalian Nek1 kinase is involved in primary cilium formation. *FEBS Lett.* **2008**, *582*, 1465−1470.
(55) Westhoff, J. H.; Giselbrecht, S.; Schmidts, M.; Schindler, S.; Beales, P. L.; Tönshoff, B.; Liebel, U.; Gehrig, J. Development of an automated imaging pipeline for the analysis of the zebrafish larval kidney. *PLoS One* **2013**, *8*, No. e82137.
(56) Sander, V.; Patke, S.; Sahu, S.; Teoh, C. L.; Peng, Z.; Chang, Y.-T.; Davidson, A. J. The small molecule probe PT-Yellow labels the renal proximal tubules in zebrafish. *Chem. Commun.* **2015**, *51*, 395−398.
(57) Christou-Savina, S.; Beales, P. L.; Osborn, D. P. S. Evaluation of Zebrafish Kidney Function Using a Fluorescent Clearance Assay. *JoVE (Journal of Visualized Experiments)* **2015**, No. e52540.
(58) Park, E. Y.; Seo, M. J.; Park, J. H. Effects of specific genes activating RAGE on polycystic kidney disease. *Am. J. Nephrol.* **2010**, *32*, 169−178.
(59) Booij, T. H.; Bange, H.; Leonhard, W. N.; Yan, K.; Fokkelman, M.; Kunnen, S. J.; Dauwerse, J. G.; Qin, Y.; van de Water, B.; van Westen, G. J. P.; Peters, D. J. M.; Price, L. S. High-throughput phenotypic screening of kinase inhibitors to identify drug targets for polycystic kidney disease. *SLAS Discov* **2017**, *22*, 974−984.
(60) Correa, R. G.; Matsui, T.; Tergaonkar, V.; Rodriguez-Esteban, C.; Izpisua-Belmonte, J. C.; Verma, I. M. Zebrafish IκB Kinase 1 Negatively Regulates NF-κB Activity. *Curr. Biol.* **2005**, *15*, 1291−1295.
(61) Li, X. Epigenetics and cell cycle regulation in cystogenesis. *Cell. Signalling* **2020**, *68*, 109509.
(62) Saigusa, T.; Bell, P. D. Molecular pathways and therapies in autosomal-dominant polycystic kidney disease. *Physiology* **2015**, *30*, 195−207.
(63) Song, X.; Di Giovanni, V.; He, N.; Wang, K.; Ingram, A.; Rosenblum, N. D.; Pei, Y. Systems biology of autosomal dominant polycystic kidney disease (ADPKD): computational identification of gene expression pathways and integrated regulatory networks. *Hum. Mol. Genet.* **2009**, *18*, 2328−2343.
(64) Baell, J. B.; Holloway, G. A. New substructure filters for removal of pan assay interference compounds (PAINS) from screening libraries and for their exclusion in bioassays. *J. Med. Chem.* **2010**, *53*, 2719−2740.
(65) Haldi, M.; Harden, M.; D'Amico, L.; DeLise, A.; Seng, W. L. Developmental Toxicity Assessment in Zebrafish. In *Zebrafish: Methods for Assessing Drug Safety and Toxicity*, McGrath, P., Ed.; John Wiley & Sons, Inc.: Hoboken, NJ, 2012; Chapter 2, pp 15−17.
(66) Edelstein, A. D.; Tsuchida, M. A.; Amodaj, N.; Pinkard, H.; Vale, R. D.; Stuurman, N. Advanced methods of microscope control using μManager software. *Journal of Biological Methods* **2014**, No. e10.

https://dx.doi.org/10.1021/acs.jmedchem.0c02118
J. Med. Chem. XXXX, XXX, XXX−XXX